Crystallographic parameterisation of distortions in the SOD framework in the sodalite and helvite groups: An analysis in condensed normal modes of an aristotype phase

Kevin S. Knight[1,2,*]

Department of Materials Science and Engineering, University of Sheffield, Sheffield S1 3JD, U.K.

Department of Earth Sciences, The Natural History Museum, Cromwell Road, London SW15 5BD, U.K.

*Author for correspondence: Kevin Knight, Email: kevinstevenknight@gmail.com

Running headers: Mode parameterisation of Sodalite

Competing interests: The author declares none

Abstract

Crystallographic distortions in the alternating aluminium and silicon tetrahedral framework of sodalite ($Na_8Al_6Si_6O_{24}Cl_2$), and beryllium and silicon in helvite ($Mn_8Be_6Si_6O_{24}S_2$), (framework designated SOD) are described in terms of a set of condensed normal mode amplitudes and phases derived from an ideal tetrahedron of a theoretical aristotype phase. For a sodalite-structured hettotype phase in space group $P\bar{4}3n$, these normal modes transform as the irreducible representations A_1, $E(\alpha)$, $T_1(z)$ of point group $\bar{4}3m$, where to a good approximation A_1 acts as a pure breathing mode, $E(\alpha)$ as a polyhedral distortive mode and $T_1(z)$ as a rigid unit rotation about the unique $\bar{4}$ axis of the T-site under consideration. Parameterisation of the mode amplitudes in terms of low-order polynomials as a function of thermodynamic variable permits the crystal structure of sodalite-structured phases to be accurately interpolated at intermediate values of the thermodynamic variable. Published data for the high temperature behaviour of sodalite have been re-analysed in terms of mode amplitudes which accurately reproduce the temperature dependence of the bond lengths, bond angles and the Al - O - Si inter-polyhedral angle. Full expressions for these derived structural parameters in terms of mode amplitudes and the lattice parameter are tabulated and agree with experimental results to within one estimated standard deviation of the experimental parameter. The potential for mode decomposition in lower symmetry SOD framework crystal structures is illustrated by deriving an aristotype structure for tugtupite ($Na_8Al_2Be_2Si_8O_{24}Cl_2$) at room temperature in space group $I\bar{4}$.

Keywords: sodalite, danalite, SOD framework, crystal structure, mode decomposition

Introduction

The crystal structure of sodalite ($Na_8Al_6Si_6O_{24}Cl_2$) and the isostructural mineral helvine ($Mn_8Be_6Si_6O_{24}S_2$) were first solved by Pauling (1930) following earlier determinations of the space group $P\bar{4}3n$ by Barth (1926) and Gottfried (1927), and comparisons of the X-ray powder diffraction patterns of haüyne ($(Na, Ca, K)_{4\text{-}8}Al_6Si_6(O,S)_{24}(SO_4, Cl)_{1\text{-}2}$), nosean ($(Na_8Al_6Si_6O_{24}(SO_4)\cdot H_2O$), sodalite and lazurite ($(Na, Ca)_{7\text{-}8}Al_6Si_6O_{24}(SO_4, S, Cl)_2\cdot H_2O$) with synthetic ultramarine (Jaeger et al. 1927, Jaeger 1929). More recently, refinement of the crystal structure of sodalite at ambient temperature has been reported by Löns and Schulz (1967) and Hassan and Grundy (1984), and at high temperatures, by McMullan et al. (1996) using neutron single crystal diffraction, and by Hassan et al. (2004), using synchrotron powder diffraction. Other mineral species such as danalite ($Fe_8Be_6Si_6O_{24}S_2$) were recognised to be isostructural with sodalite and helvine and the crystal structure of danalite was refined at ambient temperature by Hassan and Grundy (1985), and at high temperatures, by Antao et al. (2003).

The sodalite structure type is characterised by an ordered alternating framework of AlO_4 and SiO_4 tetrahedra consistent with Loewenstein's rules (Loewenstein, 1954), whose nodes lie at the vertices of a close-packed truncated octahedra (Pauling, 1930; Deer et al. 2004; Smith, 1982; O'Keeffe and Hyde, 1996; Fischer and Bauer, 2009). The cubo-octahedral cages are bounded by six rings of four tetrahedra parallel to {100} and eight rings of six tetrahedra parallel to {111}. The sodium ions lie on three-fold axes adjacent to the six-membered rings and may be considered to be four-fold coordinated to one chlorine ion and three oxygen atoms, or seven-fold coordinated to a further set of three oxygen atoms. This latter set is at a distance not always considered to be a bonded

interaction (~3.1 Å), but have been deemed to play an important role in the thermal evolution on the sodalite crystal structure (Hassan et al., 2004). The chlorine anions are sited at the centre of the truncated octahedra and are bonded to four sodium cations in a tetrahedral coordination. The crystal structure of sodalite at ambient temperature (Hassan and Grundy, 1984) is illustrated in Figure 1: the topology of the framework has been designated SOD in the database of zeolite structures (http://www.iza-structure.org/databases/).

Pauling (1930) recognised the inherent three-dimensional flexibility of the sodalite framework structure, with the rigid corner-shared tetrahedra having the ability to tilt (rotate) against each other through the bridging oxygen atoms. In a manner similar to the well-studied perovskite-structured family (Howard and Stokes, 2004), the flexibility of the SOD framework coupled with the potential to order chemically distinct cations on the tetrahedral sites permits a wide variety of symmetry descents from the most symmetric topology. These have recently been reviewed by Fischer and Bauer (2009) using group theory with the concept of Bärnighausen trees (Bärnighausen, 1975; Müller, 2013); a similar, more rigorous analysis using isotropy subgroups (Stokes and Hatch, 1988) has yet to be attempted.

The highest symmetry that can be exhibited by the SOD framework topology with a single tetrahedral site (T-site) can be described in space group $Im\bar{3}m$ and this was believed to be shown by the crystal structure of pure silica sodalite (Richardson et al., 1988), although subsequent work has shown this phase to be rhombohedral in space group $R\bar{3}$ (King et al., 2009). In space group $Im\bar{3}m$ the T-sites are not permitted to tilt relative to each other, and providing the T-sites remain close to tetrahedral geometry, it represents the fully expanded SOD topology (Taylor, 1983, 1984). Reduction in space group symmetry via condensation of a mode with irreducible representation Γ_2^- (Stokes and Hatch, 1988) results in a denser arrangement in space group $I\bar{4}3m$ with a single T-site and where tetrahedral tilting is permitted. The transformation from $Im\bar{3}m$ to $I\bar{4}3m$ does not involve either a change in lattice basis nor an associated translation of the space group origin and the SOD topology is retained. Alternatively, an ordering of the twelve T-sites into two groups of six mediated by the scalar irreducible representation H_2^+ (Stokes and Hatch, 1988) reduces the space group symmetry from $Im\bar{3}m$ to $Pm\bar{3}n$ with no lattice basis change or origin translation. Tilting of the constituent tetrahedra is not permitted in this symmetry lowering of the SOD framework. Consideration of the space group $Im\bar{3}m$ shows that the space group of the sodalite structure-type, $P\bar{4}3n$, is not an isotropy subgroup of $Im\bar{3}m$, however, $P\bar{4}3n$ is an isotropy subgroup of $I\bar{4}3m$ associated with the condensation of a mode with irreducible representation H_2 (Stokes and Hatch, 1988). This mode is associated with the loss of body-centring translations (Bradley and Cracknell, 1972), and, as a result, there are two symmetry-independent T-sites as in space group $Pm\bar{3}n$. Furthermore, space group $P\bar{4}3n$ is an isotropy subgroup of $Pm\bar{3}n$ via the condensation of a mode with symmetry Γ_2^- . Once again, these transformations are associated without origin shift or change in lattice basis. Under the Landau and Lifschitz conditions (Stokes and Hatch, 1988), hypothetical structural phase transitions from $Im\bar{3}m$ - $I\bar{4}3m$, $Im\bar{3}m$ - $Pm\bar{3}n$, $I\bar{4}3m$ - $P\bar{4}3n$ and $Pm\bar{3}n$ - $P\bar{4}3n$ are all permitted to be second order.

Further theoretical evidence for the intrinsic flexibility of the SOD framework has been afforded by the analysis of the rigid unit modes (RUMs) supported by the sodalite-structure (Hammonds et al. 1996; Dove et al., 2007). For the SOD topology in space groups $Im\bar{3}m$ and $I\bar{4}3m$

there is at least one RUM per wave vector in reciprocal space. However, in the sodalite-structured phase in space group $P\bar{4}3n$, this is no longer found to be the case (Dove et al., 2007), however high densities of RUMs exist in this space group. RUMs in the SOD framework in space group $Pm\bar{3}n$ remain to be evaluated.

Before high temperature determinations of the crystal structure of minerals became commonplace, attempts were made to predict the thermodynamic evolution of the crystal structure of framework compounds using geometric methods, pioneered in particular by Taylor and co-workers (Taylor, 1968; Taylor, 1972; Taylor, 1975; Taylor and Henderson, 1978; Dempsey and Taylor, 1980; Beagley et al., 1982; Taylor, 1983; Taylor, 1984). For the sodalite-structured phases, the O – O edges from the two symmetry independent tetrahedra that are bisected by the $\bar{4}$ axes of the tetrahedra lie in the same plane as two reciprocal lattice vectors. The smaller angle that each of these edges makes with a coplanar reciprocal lattice vector is averaged and has been used geometrically with the average edge distance to predict the lattice parameter (Taylor, 1972). This basic model for has been extended by Hassan and Grundy (1984) to utilise the independent edge lengths and angles, and once calibrated against a known structure, can be used predictively for other sodalite-structured phases.

If the thermodynamic-dependence of the lattice parameter of a sodalite-structured phase is known, the crystal structure at each thermodynamic state may in theory be deduced from distance least squares (DLS) modelling (Meier and Villiger, 1969), subject to weighted constraints for bond lengths and bond angles (Dempsey and Taylor, 1980). Taylor and Henderson (1978) developed a computer model that permitted the effects of changing cavity cation and anion radii on the unit cell parameter, tetrahedral tilt angles and the intra-polyhedral rotation angle to be predicted. Neither DLS nor the models of Taylor and Henderson (1978) or the later work of Beagley et al. (1982) appear to have been tested against experimental results collected at high temperature, high pressure or composition in a solid solution. In recent years, structural crystallographic data have been determined on a number of sodalite-structured phases as a function of composition in the helvine group (Antao et al., 2021), in temperature in sodalite (Hassan et al., 2004), danalite (Antao et al., 2004a) and synthetic chromate aluminate sodalite (Antao et al., 2003), and in pressure in helvine (Kudoh and Takéuchi, 1985). These data have all been interpreted in terms of conventional crystallographic analysis.

In this paper an alternative method for characterising and parameterising the SOD framework in space group $P\bar{4}3n$ is proposed in which the crystallographic coordination of the two symmetry independent T-sites is analysed in terms of condensed normal modes derived from an ideal aristotype SOD framework. The hypothesis of an aristotype as representing the highest crystallographic symmetry that can be attained, either theoretically or experimentally, from a lower symmetry phase has underpinned many studies of structural phase transitions (Buerger, 1947, 1961; Megaw, 1973). The lower symmetry phase(s), the hettotype(s) (Megaw, 1973) are related as isotropy subgroups of the aristotype space group (Stokes and Hatch, 1988). Applying the concept of an aristotype within a single phase with crystallographic degrees of freedom is significantly less common, and is predicated upon the structural degrees of freedom permitting an ideal polyhedral geometry. Examples where this has been successfully carried out are the framework structure of leucite (Knight and Henderson, 2019) and the crystal structure of cubic garnets (Knight, 2019). In the former case, the crystal structure may be thought of as a true aristotype in the sense of Megaw (1973), in the latter case the crystal structure should be considered to be prototypic, as the deduced crystal structure, whilst topologically correct, is crystal-chemically implausible (Knight, 2019). Despite this apparent setback, the normal mode decomposition derives correct bond lengths and angles and has shown, for the first time, that the octahedral site as well as the tetrahedral site in garnet undergoes a rigid body rotation. For the SOD

topology a set of oxygen fractional coordinates are sought that permit ideal tetrahedral geometry to define the aristotype phase. Displacement vectors from the aristotype to the hettotype phase are decomposed into normal mode amplitudes and phases for a set of symmetry adapted basis vectors that are consistent with the point group symmetry of the hettotype T-sites. The methodology is demonstrated using a crystal structure in space group $P\bar{4}3n$ at a fixed thermodynamic state before being extended to crystal structures in the same space group that vary as a function of thermodynamic variable. The results of sodalite at high temperature (Hassan et al., 2004) are re-evaluated to illustrate the procedure.

Defining aristotype crystal structures in space groups $Im\bar{3}m$, $Pm\bar{3}n$, $I\bar{4}3m$ and $P\bar{4}3n$

In the discussion developed below, symmetry descent to the space groups that permit two tetrahedral sites ($Pm\bar{3}n$ and $P\bar{4}3n$) is treated as if these sites were fully ordered. This argument is used for simplicity but it should be noted that any degree of partial order that differentiates the two tetrahedral sites would be equally acceptable. The subsequent section that deals with the methodology of mode decomposition of the two tetrahedral sites in the SOD framework in space group $P\bar{4}3n$ is also treated in the same manner, but again, the analysis is equally valid for partially ordered tetrahedral sites.

Space group $Im\bar{3}m$

Fischer and Bauer (2009) considered the SOD framework in space group $Im\bar{3}m$ to represent the aristotype phase of a sodalite-structured phase, however, this ignores the fact that the oxygen coordinate has a single degree of freedom (x, x, 1/2) that permits non-ideal tetrahedral bond angle geometry. The tetrahedral site in space group $Im\bar{3}m$ in Wyckoff position 12*d* exhibits point group symmetry $\bar{4}m2$, and as a result of the tetragonal point group symmetry, the four T-site - anion bond lengths are constrained to have equal magnitudes. This point group symmetry also permits two independent tetrahedral bond angles of multiplicities two and four, with the unique roto-inversion axis of the point group bisecting the bond angles of multiplicity two. For the T-site at (1/4, 0, 1/2) the roto-inversion axis is directed along [-1 0 0] (or equivalently [1 0 0]) as illustrated in Figure 2a. The bonded anions lie on Wyckoff positions 24*h* with point group symmetry *mm*2 and a single degree of structural freedom (x) as detailed in Table 1. To derive the true aristotype crystal structure it is necessary to find a real value of x that results in the two independent bond angles becoming equal. The point group symmetry of the T-site is therefore raised from $\bar{4}m2$ to $\bar{4}3m$, and ideal tetrahedral geometry is therefore realised. This can be determined by equating the inner products of the bond vectors **r1.r2** with **r1.r3** and solving the resultant quadratic equation $x^2 - x + 1/8 = 0$. Of the two possible solutions, only the solution $x = 1/2 - 1/\sqrt{8}$ (~0.14645) results in a crystallographically acceptable bond length. The fractional coordinates of the anion with $x = 1/2 - 1/\sqrt{8}$ defines the true aristotype SOD framework structure in this space group with a T – O bond length of $\frac{3a}{4}\sqrt{1-\frac{\sqrt{8}}{3}}$ Å , intra-polyhedral angle (T – O – T) $\cos^{-1}(-\sqrt{8}/3)$ (~160.529°) and tetrahedral volume of $(a^3/24)(3 - \sqrt{8})^{1.5}$ Å^3 (where a is the lattice parameter).

Space group $Pm\bar{3}n$

The loss of mirror plane lying at x, x, z and the reduction in symmetry associated with the four-fold rotation axis along 0, 0, z becoming a two-fold rotation axis (and symmetry equivalents under $\bar{3}$ point group symmetry) reduces the space group symmetry from $Im\bar{3}m$ to $Pm\bar{3}n$. The descent in symmetry results in the single T-site in $Im\bar{3}m$ in Wyckoff site 12d becoming two tetrahedral sites with Wyckoff positions 6c (1/4, 0, 1/2) and 6d (1/2, 0, 3/4) but retaining the site point group symmetry $\bar{4}m2$ (noting that the Wyckoff notation for the two sites is the reverse of that designated for space group $P\bar{4}3n$). The unique roto-inversion axis lies parallel to [-1 0 0] (equivalently [1 0 0]) for the site 6c at (1/4, 0, 1/2), and parallel to [0 0 -1] (equivalently [0 0 1]) for site 6d at (1/2, 0, 3/4). The coordinating anions lie on a mirror plane with Wyckoff position 24 k (x, y, 1/2) as listed in Table 1, with the difference in x and y permitting different bond lengths to be associated with the two independent T-sites. The identical, tetragonal point group symmetry for both T-sites ensures that the four bond lengths associated with either site are identical in length and have two sets of bond angles of multiplicities two and four. The unique roto-inversion axis bisects the bond angles of multiplicity two and the local geometry is illustrated in Figure 2b. Defining the aristotype sodalite structure for this space group as the fractional coordinate of the anion that results in ideal tetrahedral bond angles at both T-sites, a solution is sought where **r1.r2/|r1.r2|** = **r1.r3/|r1.r3|**, **r5.r6/|r5.r6|**, **r5.r7/|r5.r7|** = -1/3. Equating **r1.r2/|r1.r2|** = **r5.r6/|r5.r6|** finds the single acceptable solution $x = y$, and equating **r1.r2/|r1.r2|** = **r1.r3/|r1.r3|** results in the quadratic equation $x^2 - x + 1/8 = 0$ with solution $x = 1/2 - 1/\sqrt{8}$. The aristotype structure is therefore identical to that derived for space group $Im\bar{3}m$ with a single T – O bond length of $\frac{3a}{4}\sqrt{1-\frac{\sqrt{8}}{3}}$ Å , intra-polyhedral angle $\cos^{-1}(-\sqrt{8}/3)$ and tetrahedral volume of $(a^3/24)(3 - \sqrt{8})^{1.5}$ Å^3.

Space group $I\bar{4}3m$

The tetrahedral site in space group $I\bar{4}3m$ in Wyckoff position 12d exhibits point group symmetry $\bar{4}$, and as in space group $Im\bar{3}m$, the four T-site - anion bond lengths are constrained by the tetragonal symmetry to have equal magnitudes. The point group symmetry permits two independent tetrahedral bond angles of multiplicities two and four with the unique roto-inversion axis bisecting the bond angles of multiplicity two. The orientation of the roto-inversion axis associated with the T-site at (1/4, 0, 1/2) is unchanged from that in space group $Im\bar{3}m$, as illustrated in Figure 2c. The bonded anions lie on a mirror plane in Wyckoff positions 24g and two degrees of structural freedom (x, x, z) as detailed in Table 1. To derive an aristotype structure, values of x and z are therefore sought that result in the two independent bond angles becoming equal. The point group symmetry of the T-site is then raised from $\bar{4}$ to $\bar{4}3m$ and ideal tetrahedral geometry is realised. Equating the inner products of the bond vectors **r1.r2** with **r1.r3** results in the polynomial equation $x^2 - x - z^2 + z - 1/8 = 0$ indicating that an infinite set of solutions are possible. The range of solutions is clearly reduced by the constraint of an acceptable bond length for the T-site and anion under consideration, but despite this constraint, there is not a unique aristotype framework structure in space group $I\bar{4}3m$. For chosen z and calculated x, the aristotype T – O bond length is $\sqrt{3}a(\Delta - 1/4)$, intra-polyhedral angle $\cos^{-1}((5/4 + 3z^2 – 3z – 3\Delta/2)/(21/16 + 3z^2 – 3z – 3\Delta/2))$ and tetrahedral volume $((8a^3)/(9\sqrt{3}))(21/16 + 3z^2 – 3z – 3\Delta/2)^{3/2}$ with Δ defined as $(3/8 - z + z^2)^{1/2}$. Analysis of the intra-polyhedral angle function shows it to exhibit a single maximum at $z = 0.5$ for acceptable values of z. The solution derived for space group $Im\bar{3}m$, $x = 1/2 -$

$1/\sqrt{8}$, $z = 1/2$, satisfies the polynomial equation above and therefore represents one of the many aristotype framework structures for space group $I\bar{4}3m$. A mineralogical example of the SOD framework within this space group is afforded by the phase bicchulite ($Ca_8Al_8Si_4O_{24}(OH)_8$) (Sahl, 1980).

Space group $P\bar{4}3n$

The symmetry lowering in space group $P\bar{4}3n$ from space group $I\bar{4}3m$ associated with the loss of body-centring translations gives rise to two tetrahedral sites with 6-fold multiplicity and point group symmetry $\bar{4}$, as shown in Figure 2d. The Wyckoff site 6*d* at (1/4, 0, 1/2) is identical in character to the position (1/4, 0, 1/2) in Wyckoff site 12*d* associated with space groups $Im\bar{3}m$ and $I\bar{4}3m$, and 6*c* in space group $Pm\bar{3}n$. In an identical manner to Wyckoff site 6*d* in space group $Pm\bar{3}n$, the symmetry independent T-site at Wyckoff position 6*c* (1/2, 0, 3/4) is associated with the roto-inversion axis directed along [0 0 -1] (or equivalently [0 0 1]), and, as in position 6*d*, bisects the bond angle with two-fold multiplicity. Anion fractional coordinates are in the general equivalent position in Wyckoff site 24*i* as listed in Table 1. Making the definition that the aristotype in this space group is the framework structure in which both T-sites are ideal tetrahedra with identical bond lengths, there are additional simultaneous constraints that have to be applied to determine any possible solution. Firstly, the bond length equivalence implies **r1.r1 = r5.r5**, and secondly, the bond angle equivalence requires that **r1.r2/|r1.r2| = r1.r3/|r1.r3|**, **r5.r6/|r5.r6|**, **r5.r7/|r5.r7|**. Expanding and equating the first and second inner product shows the bond length equivalence results in the equality $1/2(y - x) = 0$ i.e. $x = y$, and substituting this solution into the bond angle constraints results in the identical polynomial equation as found for the space group $I\bar{4}3m$; $x^2 - x - z^2 + z - 1/8 = 0$. Hence, there are an infinite set of solutions (x, x, z), the valid solutions being constrained by the bond length requirement. The expressions for the T – O bond length, T – O – T intra-polyhedral angle and tetrahedral volume that were derived for space group $I\bar{4}3m$ are identical for the potential aristotype phases of space group $P\bar{4}3n$ **.** The solution derived for space groups $Im\bar{3}m$, $Pm\bar{3}n$ and $I\bar{4}3m$, $x = y = 1/2 - 1/\sqrt{8}$, $z = 1/2$, satisfies the polynomial equation above and therefore represents one of the many potential aristotype framework structures for space group $P\bar{4}3n$.

Mode decomposition in space group $P\bar{4}3n$

The methodology to be applied to the SOD framework is to compare the observed framework structure (hettotype) with an associated aristotype framework structure, and to analyse the distortions therefrom (the displacement vectors between identically labelled atoms in the two crystal structures) in terms of condensed normal modes of the ideal tetrahedral isolated TO_4 'molecule'. To achieve this it is necessary to define a local orthonormal basis (**i**, **j**, **k**) that brings the aristotype tetrahedron in absolute coordinates into an orientation that matches the basis to the constituent symmetry elements of the point group $\bar{4}3m$. In this case, the orthonormal basis is parallel to the three four-fold roto-inversion axes of the ideal tetrahedron, with the T-site translated to the origin, as shown in Figure 3. The basis is chosen such that the unique $\bar{4}$ axis derived from the hettotype is parallel to **k**. In this

basis, for a cube of side 2*l*, the absolute coordinates of the TO_4 tetrahedron in the aristotype are T (0, 0, 0), O1 (-*l*, -*l*, *l*), O2 (*l*, *l*, *l*), O3 (*l*, -*l*, -*l*) and O4 (-*l*, *l*, -*l*).

The normal modes that are active in the parameterisation of the observed SOD framework are those of point group $\bar{4}3m$ that are consistent with the point group symmetry of the hettotype phase, $\bar{4}$. It should be noted that, in general, the zero frequency modes of rigid body rotation and translation, that are discounted in normal mode analysis for free molecules (Bishop, 1972; Decius and Hexter, 1977), may be present as frozen modes in a static crystal structure mode decomposition.

The three components of molecular displacements from each atom of the isolated TO_4 tetrahedron form a fifteen-dimensional vector basis of a reducible fifteen-dimensional representation (Γ_{15}) of point group $\bar{4}3m$ (Bishop, 1972; El-Betanouny and Wooten, 2008). This representation is reducible using standard group theoretical methods (Bishop, 1972; Ladd, 2014) to yield the direct sum of irreducible representations.

$$\Gamma_{15} = A_1 \oplus E \oplus 3T_2 \oplus T_1 \quad (1)$$

Consideration of the character table of point group $\bar{4}3m$ shows that only the displacements that transform as the irreducible representations A_1, E and T_1 are consistent with point group $\bar{4}$ (Bishop, 1972; Ladd, 2014; El-Betanouny and Wooten, 2008), and furthermore, these only involve displacements of the anions. Symmetry-adapted basis-vectors were calculated for the (**i**, **j**, **k**) basis using standard projection operator methods (Ladd, 2014; El-Betanouny and Wooten, 2008), using results from the Bilbao Crystallographic Server (Aroyo et al., 2006), noting only one of the basis vectors that transform as the irreducible representations E and T_1 is consistent with point group symmetry $\bar{4}$ with the unique roto-inversion axis parallel to **k**. These active modes are designated $E(\alpha)$ and $T_1(z)$ for convenience. The symmetry-adapted basis-vectors in the (**i**, **j**, **k**) basis are illustrated in Figure 3 where it can be seen that A_1 is a breathing mode, $E(\alpha)$ is a tetrahedral distortion mode and $T_1(z)$ is effectively a rotation around **k** for small basis vector displacements. The symmetry-adapted basis-vectors for the four anion positions are listed in Table 2. The amplitude and phase (sign) of the symmetry-adapted basis-vectors are written d1 for A_1, d2 for $E(\alpha)$ and d3 for $T_1(z)$.

Mode displacements in a crystal structure in space group $P\bar{4}3n$ at a fixed thermodynamic state

Without loss of generality, in the subsequent discussion, the aristotype SOD framework in space group $P\bar{4}3n$ is chosen to be that defined by the selection of the z coordinate ($x = 1/2 - \sqrt{z^2 - z - 3/8}$) . The methodology is equally valid for a given value of x, where the related z coordinate is calculated as $1/2 - \sqrt{x^2 - x - 1/8}$. The choice of which coordinate to use to define the aristotype crystal structure is arbitrary, however, using the z coordinate for the anion O1 at (~1/2 - 1/√8, ~1/2 - 1/√8, ~1/2), or the average of the x and y coordinates of the same atom to define the aristotype x would be sensible options. For comparison with an actual or hypothetical crystal structure in space group $Im\bar{3}m$, setting z = 1/2 would be the best choice. In the subsequent analysis, the two tetrahedral sites are taken separately; site 6*d* is described in detail, site 6*c* simply follows in an analogous manner.

Transformation of the aristotype at site 6*d* to the final orthonormal basis is achieved in three steps. Firstly, by a translation of the entire TO_4 group by (1/4, 0, 1/2) bringing the site 6*d* to the origin

of the orthonormal crystallographic space. Secondly, an intermediate basis $\mathbf{e_i}$ is defined by the bond vectors illustrated in Figure 2d as $\mathbf{e_1} = \frac{\mathbf{r2}-\mathbf{r1}}{|\mathbf{r2}-\mathbf{r1}|}$, $\mathbf{e_2} = \frac{\mathbf{r4}-\mathbf{r3}}{|\mathbf{r4}-\mathbf{r3}|}$, $\mathbf{e}_3 = \mathbf{e}_1 \times \mathbf{e}_2$ thus bringing the unique $\bar{4}$ axis parallel to $\mathbf{e_3}$; transformation matrix **M1**. For convenience and ease of subsequent matrix manipulations, the parameter S is defined as $S = \sqrt{(-1+2\Delta)^2 + (1-2z)^2}$, Δ as defined earlier.

$$\mathbf{M1} = \begin{pmatrix} 0 & \frac{-1+2\Delta}{S} & \frac{1-2z}{S} \\ 0 & \frac{1-2z}{S} & \frac{1-2\Delta}{S} \\ -1 & 0 & 0 \end{pmatrix} \quad (2)$$

The final basis (**i**, **j**, **k**) is derived from the intermediate basis with a passive rotation of $\pi/4$ around $\mathbf{e_3}$; rotation matrix **R**.

$$\mathbf{R} = \begin{pmatrix} \frac{1}{\sqrt{2}} & \frac{-1}{\sqrt{2}} & 0 \\ \frac{1}{\sqrt{2}} & \frac{1}{\sqrt{2}} & 0 \\ 0 & 0 & 1 \end{pmatrix} \quad (3)$$

As the both matrix **M1** and the rotation matrix **R** are orthogonal, their product is therefore also orthogonal, and its inverse is the transpose of the product (Poole, 2014). The absolute coordinates of the aristotype (primed) in the **i**, **j**, **k** basis, in terms of its fractional coordinates in the orthonormal crystallographic basis, is therefore given by the product of the matrices (a**T1** = a**RM1**)

$$\begin{pmatrix} x' \\ y' \\ z' \end{pmatrix}_{\mathbf{i},\mathbf{j},\mathbf{k}} = a \begin{pmatrix} 0 & \frac{\sqrt{2}(\Delta+z-1)}{S} & \frac{\sqrt{2}(\Delta-z)}{S} \\ 0 & \frac{\sqrt{2}(\Delta-z)}{S} & \frac{\sqrt{2}(-\Delta-z+1)}{S} \\ -1 & 0 & 0 \end{pmatrix} \begin{pmatrix} x \\ y \\ z \end{pmatrix}_{\hat{\mathbf{a}},\hat{\mathbf{b}},\hat{\mathbf{c}}} \quad (4)$$

where a is the lattice parameter of the hettotype. The coordinates of the aristotype in this basis are T (0, 0, 0), O1 (-l, -l, l), O2 (l, l, l), O3 (l, -l, -l) and O4 (-l, l, -l) where $l = a(\Delta - 1/4)$.

To determine the displacement vectors from the aristotype to the hettotype, the hettotype fractional coordinates are translated by (1/4, 0, 1/2) and then transformed by a**T1** to the new basis. Subtracting the transformed aristotype coordinates from the corresponding transformed hettotype coordinates gives the four displacement vectors **ΔOi** i = 1 - 4. If the manipulations have been carried out correctly, the four displacement vectors obey the symmetry operations of point group $\bar{4}$, for example, the displacements at **ΔO4** are related to those at **ΔO1** by the symmetry operation $\bar{4}^+$ (0, 0, z).

For the tetrahedral site 6*c*, the same sequence of operations is carried out, with the translation vector in this case being (1/2, 0, 3/4), and the intermediate vector basis being defined by $\mathbf{e}_1^{'} = \frac{\mathbf{r}6 - \mathbf{r}5}{|\mathbf{r}6 - \mathbf{r}5|}$, $\mathbf{e}_2^{'} = \frac{\mathbf{r}8 - \mathbf{r}7}{|\mathbf{r}8 - \mathbf{r}7|}$, $\mathbf{e}_3^{'} = \mathbf{e}_1^{'} \times \mathbf{e}_2^{'}$; transformation matrix **M2**. The final basis (**i′**, **j′**, **k′**) is derived from the intermediate basis with a passive rotation of π/4 around $\mathbf{e}_3^{'}$. The absolute coordinates of the aristotype (primed) in the **i′**, **j′**, **k′** basis, in terms of its coordinates in the orthonormal crystallographic basis, is therefore given by the product of the matrices (*a***T2** = *a***RM2**)

$$\begin{pmatrix} x' \\ y' \\ z' \end{pmatrix}_{\mathbf{i}',\mathbf{j}',\mathbf{k}'} = \mathrm{a} \begin{pmatrix} \frac{\sqrt{2}(1-\Delta-z)}{S} & \frac{\sqrt{2}(-\Delta+z)}{S} & 0 \\ \frac{\sqrt{2}(-\Delta+z)}{S} & \frac{\sqrt{2}(-1+\Delta+z)}{S} & 0 \\ 0 & 0 & -1 \end{pmatrix} \begin{pmatrix} x \\ y \\ z \end{pmatrix}_{\hat{\mathbf{a}},\hat{\mathbf{b}},\hat{\mathbf{c}}} \quad (5)$$

where *a* is the lattice parameter of the hettotype. The coordinates of the aristotype in this basis are T (0, 0, 0), O4 (-*l*, -*l*, *l*), O6 (*l*, *l*, *l*), O7 (*l*, -*l*, -*l*) and O8 (-*l*, *l*, -*l*) where $l = a(\sqrt{8} - 1/4)$. The displacement vectors **ΔOi** i = 4, 6 - 8 follow accordingly.

Consideration of Table 2 shows the displacement vector **ΔO1** is related to the amplitudes and phase of the symmetry-adapted basis-vectors **di** via the matrix **DO1** where

$$\begin{pmatrix} \Delta \mathrm{O1}x \\ \Delta \mathrm{O1}y \\ \Delta \mathrm{O1}z \end{pmatrix} = \begin{pmatrix} -1 & -1 & 1 \\ -1 & -1 & -1 \\ 1 & -2 & 0 \end{pmatrix} \begin{pmatrix} \mathrm{d1} \\ \mathrm{d2} \\ \mathrm{d3} \end{pmatrix} \quad (6)$$

and hence

$$\begin{pmatrix} \mathrm{d1} \\ \mathrm{d2} \\ \mathrm{d3} \end{pmatrix} = \begin{pmatrix} -1/3 & -1/3 & 1/3 \\ -1/6 & -1/6 & -1/3 \\ 1/2 & -1/2 & 0 \end{pmatrix} \begin{pmatrix} \Delta \mathrm{O1}x \\ \Delta \mathrm{O1}y \\ \Delta \mathrm{O1}z \end{pmatrix}. \quad (7)$$

Writing d1′, d2′ and d3′ for the amplitude and phase of the displacements of the symmetry-adapted basis-vectors associated with the 6*c* site and noting **ΔO4** shown below is given in the (**i′**, **j′**, **k′**) basis, then

$$\begin{pmatrix} \mathrm{d1}' \\ \mathrm{d2}' \\ \mathrm{d3}' \end{pmatrix} = \begin{pmatrix} -1/3 & -1/3 & 1/3 \\ -1/6 & -1/6 & -1/3 \\ 1/2 & -1/2 & 0 \end{pmatrix} \begin{pmatrix} \Delta \mathrm{O4}x \\ \Delta \mathrm{O4}y \\ \Delta \mathrm{O4}z \end{pmatrix}. \quad (8)$$

Furthermore, writing the deviation of the fractional coordinates of the hettotype anion O1 (x_h, y_h, z_h) from the aristotype as $u = x_\mathrm{h} - x$, $v = y_\mathrm{h} - x$ and $w = z_\mathrm{h} - z$ and carrying these calculations through to completion gives di and di′ directly in terms of *u*, *v*, *w*:

$$\mathrm{d1} = \frac{\sqrt{2}a}{3S}\left[\frac{-Su}{\sqrt{2}} + (1-2\Delta)v + (2z-1)w\right]$$

$$\mathrm{d2} = \frac{a}{3\sqrt{2}S}\left[\sqrt{2}Su + (1-2\Delta)v + (2z-1)w\right]$$

$$\mathrm{d3} = \frac{a}{\sqrt{2}S}\left[(2z-1)v + (1-2\Delta)w\right]$$

$$\mathrm{d1}' = \frac{\sqrt{2}a}{3S}\left[(1-2\Delta)u - \frac{Sv}{\sqrt{2}} + (2z-1)w\right]$$

$$\mathrm{d2}' = \frac{a}{3\sqrt{2}S}\left[(1-2\Delta)u + \sqrt{2}Sv + (2z-1)w\right]$$

$$\mathrm{d3}' = \frac{a}{\sqrt{2}S}\left[(2z-1)u + (1-2\Delta)w\right] \quad . (9)$$

The absolute coordinates of the two tetrahedral sites for the **i**, **j**, **k** and **i′**, **j′**, **k′** bases are listed in Table 3.

Using the normal mode amplitudes, the derived structural parameters are given by:

(i) Tetrahedral bond lengths

$$\mathrm{r1} = \sqrt{3a^2\left(\Delta - \frac{1}{4}\right)^2 + 6a\left(\Delta - \frac{1}{4}\right)\mathrm{d1} + 3\mathrm{d1}^2 + 6\mathrm{d2}^2 + 2\mathrm{d3}^2} \quad (10)$$

$$\mathrm{r5} = \sqrt{3a^2\left(\Delta - \frac{1}{4}\right)^2 + 6a\left(\Delta - \frac{1}{4}\right)\mathrm{d1}' + 3\mathrm{d1}'^2 + 6\mathrm{d2}'^2 + 2\mathrm{d3}'^2} \quad (11)$$

(ii) Tetrahedral edge lengths of multiplicity two

$$\sqrt{8}\sqrt{a^2\left(\Delta - \frac{1}{4}\right)^2 + \mathrm{d1}^2 + \mathrm{d2}^2 + \mathrm{d3}^2 + 2a\left(\Delta - \frac{1}{4}\right)(\mathrm{d1} + \mathrm{d2}) + 2\mathrm{d1}\mathrm{d2}} \quad (12)$$

$$\sqrt{8}\sqrt{a^2\left(\Delta - \frac{1}{4}\right)^2 + \mathrm{d1}'^2 + \mathrm{d2}'^2 + \mathrm{d3}'^2 + 2a\left(\Delta - \frac{1}{4}\right)(\mathrm{d1}' + \mathrm{d2}') + 2\mathrm{d1}'\mathrm{d2}'} \quad (13)$$

(iii) Tetrahedral edge lengths of multiplicity four

$$\sqrt{8}\sqrt{a^2\left(\Delta - \frac{1}{4}\right)^2 + \mathrm{d1}^2 + \frac{5}{2}\mathrm{d2}^2 + \frac{1}{2}\mathrm{d3}^2 + a\left(\Delta - \frac{1}{4}\right)(2\mathrm{d1} - \mathrm{d2}) - \mathrm{d1}\mathrm{d2}} \quad (14)$$

$$\sqrt{8}\sqrt{a^2\left(\Delta - \frac{1}{4}\right)^2 + \mathrm{d1}'^2 + \frac{5}{2}\mathrm{d2}'^2 + \frac{1}{2}\mathrm{d3}'^2 + a\left(\Delta - \frac{1}{4}\right)(2\mathrm{d1}' - \mathrm{d2}') - \mathrm{d1}'\mathrm{d2}'} \quad (15)$$

(iv) Bond angles of multiplicity two

$$\cos^{-1}\left(\frac{-a^2\left(\Delta-\frac{1}{4}\right)^2-2a\left(\Delta-\frac{1}{4}\right)(\mathrm{d1}+4\mathrm{d2})-\mathrm{d1}^2+2\mathrm{d2}^2-2\mathrm{d3}^2-8\mathrm{d1d2}}{\mathrm{r1}^2}\right) \quad (16)$$

$$\cos^{-1}\left(\frac{-a^2\left(\Delta-\frac{1}{4}\right)^2-2a\left(\Delta-\frac{1}{4}\right)(\mathrm{d1}'+4\mathrm{d2}')-\mathrm{d1}'^2+2\mathrm{d2}'^2-2\mathrm{d3}'^2-8\mathrm{d1}'\mathrm{d2}'}{\mathrm{r5}^2}\right) \quad (17)$$

(v) Bond angles of multiplicity four

$$\cos^{-1}\left(\frac{-a^2\left(\Delta-\frac{1}{4}\right)^2-2a\left(\Delta-\frac{1}{4}\right)(\mathrm{d1}-2\mathrm{d2})-\mathrm{d1}^2-4\mathrm{d2}^2+4\mathrm{d1d2}}{\mathrm{r1}^2}\right) \quad (18)$$

$$\cos^{-1}\left(\frac{-a^2\left(\Delta-\frac{1}{4}\right)^2-2a\left(\Delta-\frac{1}{4}\right)(\mathrm{d1}'-2\mathrm{d2}')-\mathrm{d1}'^2-4\mathrm{d2}'^2+4\mathrm{d1}'\mathrm{d2}'}{\mathrm{r5}^2}\right) \quad (19)$$

(vi) The intra polyhedral angle by

$$\cos^{-1}\left(\left(\frac{1}{\mathrm{r1r5}}\right)(\mathrm{A}+\mathrm{B}+\mathrm{C})\right)$$

$$\mathrm{A}=\frac{a^2\left(\Delta-\frac{1}{4}\right)}{\sqrt{8}S}\left[3\sqrt{8}\Delta S+2\Delta-2\sqrt{2}S-1\right] \quad . (20)$$

$$\mathrm{B}=a\left[\mathrm{d1}\left(3\left(\Delta-\frac{1}{4}\right)+\left(\frac{3\sqrt{8}\Delta S+2\Delta-\sqrt{8}S-1}{\sqrt{8}S}\right)\right)+\mathrm{d2}\left(\frac{2\Delta+\sqrt{2}S-1}{\sqrt{8}S}\right)+\mathrm{d3}\left(\frac{1-2z}{\sqrt{8}S}\right)\right]$$

$$\mathrm{C}=3\mathrm{d1}^2+6\mathrm{d2}^2+2\mathrm{d3}^2$$

Utilising crystallographic results from sodalite (Hassan and Grundy), a = 8.882 Å, Al (1/4, 0, 1/2), Si (1/2, 0, 3/4) and O (0.1390, 0.1494, 0.4383), then with the aristotype z = 0.4383 (x = 0.14110, Δ = 0.3589), d1 = 0.03806 Å, d2 = 0.00969 Å, d3 = -0.02082 Å, d1′ = -0.03263 Å, d2′ = 0.02053 Å and d3′ = 0.00529 Å. The observed (recalculated) bond lengths and bond angles are compared with the calculations from mode decomposition in Table 4 where the agreement is found to be close to exact.

The aristotype bond length is given by $\sqrt{3}a(\Delta - 1/4)$ (1.6753 Å), the calculated quadratic elongation and tetrahedral angle variance (Robinson et al., 1971) of the AlO_4 site (6*d*) in sodalite are 1.0008 and 1.41°^{2} respectively. At the SiO_4 site (6*c*), the corresponding parameters are 1.0025 and 7.49°^{2}. Approximating the ratio of the observed bond lengths to the aristotype bond length as a binomial expansion to first order, the dominant term in the expansion is found to be d1(′)/$a(\Delta - 1/4)$.

Hence, with the choice of the aristotype z fractional coordinate made in this analysis, the effect of the amplitude and phase of d1 and d1′ is to increase the Al – O bond length from the aristotype value with the converse found for the Si – O bond length as d1 > 0 and d1′ < 0. The bond length changes are in agreement with the observed Al – O and Si – O bond lengths in sodalite, and to a good approximation in this aristotype definition, d1(′) act as pure breathing modes. The polyhedral distortion that transforms as the irreducible representation $E(\alpha)$ is associated with the positive mode amplitudes d2 and d2′, where d2′ > d2, consistent with the larger quadratic elongation and tetrahedral angle variance in the SiO_4 group in sodalite. The AlO_4 tetrahedron is rotated -0.44° away from the aristotype orientation around **k**, the SiO_4 tetrahedron rotates in the opposite direction by 0.11° ($\tan\varphi(') = \frac{d3(')}{a\left(\Delta - 1/4\right)}$) as d3 < 0 and |d3| > d3′. Note that this interpretation as a rotation about the unique axis is only valid in small displacements of d3 and d3′ i.e. in this case, setting aristotype z to be the z fractional coordinate for the anion at (~1/2 - 1/√8, ~1/2 - 1/√8, ~1/2).

The analysis presented above is equally valid for the other three space groups discussed. For example, if the crystal structure of bicchulite (Sahl, 1980) in space group $I\bar{4}3m$ is analysed with the undifferentiated tetrahedral site (T) at (0.25, 0.50, 0.0) and the oxygen anion (O) at (0.1407, 0.1407, 0.4220), mode decomposition yields d1(′) = 1.873 × 10^{-3} Å, d2(′) = 0.0131 Å, and d3(′) = -8.4631.873 × 10^{-3} Å, for aristotype z = 0.4220. The calculated and observed bond lengths and angles are T - O = 1.7164 Å calc., 1.716(1) Å obs., O - T - O (multiplicity 2) = 111.615 ° calc., 111.6(1) ° obs. (typographical error in Table 2 of Sahl (1980) reads 111.9 °), O - T - O (multiplicity 4) = 108.410 ° calc., 108.4(1) ° obs., T - O - T = 130.712 ° calc. and obs.. See later section for discussion of mode and crystallographic degrees of freedom in this space group.

Mode displacements in a crystal structure in space group $P\bar{4}3n$ as a function of thermodynamic variable

The methodology detailed above is particularly advantageous in the study of the SOD framework as a function of thermodynamic variable such as temperature, pressure, or composition in a solid solution. In these cases, the aristotype is defined at a fixed value of the thermodynamic variable, and the evolving crystal structure as a function of this variable is derived in terms of the mode amplitudes. The basis of the analysis is the observation that an aristotype in space group $P\bar{4}3n$ may be defined for any set of fractional coordinates (x, x, z) where x and z satisfy the polynomial expression $x^2 - x - z^2 + z - 1/8 = 0$. In mode decomposition as a function of thermodynamic variable, the optimal choice of aristotype would be therefore be based on the z coordinate of the anion with fractional coordinates (~1/2 - 1/√8, ~1/2 - 1/√8, ~1/2) at ambient pressure, for a study in pressure, the lowest temperature, for a study in temperature, or an end member, for a study in composition. The aristotype is transformed to absolute coordinates, as shown in the previous section, with lattice parameter a_a and the hettotype is transformed identically, but in this case using its own lattice parameter a. The displacement vectors from identically labelled anions in the aristotype and hettotype are mode decomposed using the matrices shown earlier. The expressions for the bond lengths and bond angles are unchanged from those listed earlier, only the lattice parameter a requires replacing with a_a. The intra-polyhedral angle, however, is a more complex function than shown earlier, as the calculation involves taking into account the requirement that the site 6c has to be transformed into the **i**, **j**, **k** basis. Writing $\Delta a = a - a_a$, the intra-polyhedral angle is given by:

$$\cos^{-1}\left(\left(\frac{1}{\mathrm{r1r5}}\right)(\mathrm{A}+\mathrm{B}+\mathrm{C}+\mathrm{D})\right)$$

$$\mathrm{A}=\frac{{a_\mathrm{a}}^2\left(\Delta-\frac{1}{4}\right)}{\sqrt{8}S}\left[3\sqrt{8}\Delta S+2\Delta-2\sqrt{2}S-1\right]$$

$$\mathrm{B}=a_\mathrm{a}\left[\left(\frac{3\sqrt{8}\Delta S+2\Delta-\sqrt{8}S-1}{\sqrt{8}S}\right)\mathrm{d}_1+\left(\frac{2\Delta+\sqrt{2}S-1}{\sqrt{8}S}\right)\mathrm{d}_2+\left(\frac{1-2z}{\sqrt{8}S}\right)\mathrm{d}_3\right] \quad (21)$$

$$\mathrm{C}=a_a\left(\Delta-\frac{1}{4}\right)\left[3\mathrm{d}_1+\frac{\Delta a}{\sqrt{8}S}\left(2\Delta-1-\frac{S}{\sqrt{2}}\right)\right]$$

$$\mathrm{D}=3{\mathrm{d}_1}^2+6{\mathrm{d}_2}^2+2{\mathrm{d}_3}^2-\frac{\Delta a}{\sqrt{8}S}\left[\left(-2\Delta+1+\frac{S}{\sqrt{2}}\right)\mathrm{d}_1+\left(-2\Delta+1-\sqrt{2}S\right)\mathrm{d}_2+\left(2z-1\right)\mathrm{d}_3\right]$$

For the aristotype, where $\Delta a = 0$, the expression reduces to that shown previously for mode decomposition at a fixed thermodynamic state.

Taylor (1972) has defined the polyhedral tilt angles ($\varphi_{6c,d}$) for the two T-sites as the angle between a tetrahedral edge and the closest of the two reciprocal lattice vectors which are co-planar with the edge in question. The change in $\varphi_{6c,d}$ is a fundamental structural response to a change in thermodynamic state, and since it is related to the anion fractional coordinates, it can be described as a function of condensed mode amplitudes and phases. For a hettotype phase, the two polyhedral tilt angles generally have different magnitudes, however, in the aristotype phase these angles are identical (φ) and additional mode-related rotational term are required to be included to correctly evaluate the polyhedral tilt angles at the two T-sites.

$$\varphi_{6c,d}=\varphi\pm\Delta\varphi_{6c,d}$$

$$\varphi=\cos^{-1}\left(\frac{1-2\Delta}{\sqrt{(1-2\Delta)^2+(1-2z)^2}}\right)$$

$$\Delta\varphi_{6c}=\cos^{-1}\left(\frac{a_\mathrm{a}(\Delta-1/4)+\mathrm{d1}'+\mathrm{d2}'}{\sqrt{{a_\mathrm{a}}^2(\Delta-1/4)^2+2a_\mathrm{a}(\Delta-1/4)(\mathrm{d1}'+\mathrm{d2}')+\mathrm{d1}'^2+\mathrm{d2}'^2+\mathrm{d3}'^2+2\mathrm{d1}'\mathrm{d2}'}}\right) \quad (22)$$

$$\Delta\varphi_{6d}=\cos^{-1}\left(\frac{a_\mathrm{a}(\Delta-1/4)+\mathrm{d1}+\mathrm{d2}}{\sqrt{{a_\mathrm{a}}^2(\Delta-1/4)^2+2a_\mathrm{a}(\Delta-1/4)(\mathrm{d1}+\mathrm{d2})+\mathrm{d1}^2+\mathrm{d2}^2+\mathrm{d3}^2+2\mathrm{d1d2}}}\right)$$

The sign for $\Delta\varphi_{6c,d}$ is negative for $\frac{a_\mathrm{a}(\Delta-1/4)+\mathrm{d1}(')+\mathrm{d2}(')-\mathrm{d3}(')}{a_\mathrm{a}(\Delta-1/4)+\mathrm{d1}(')+\mathrm{d2}(')+\mathrm{d3}(')}\geq 1$, otherwise positive.

The temperature dependence of the crystal structure of sodalite

The methodology of mode decomposition with respect to a reference aristotype phase is illustrated using the temperature dependence of the crystal structure of sodalite derived from profile fitting of synchrotron X-ray diffraction data (Hassan et al., 2004). It should be noted that the tabulated bond lengths and bond angles are not consistent with the fractional coordinates and lattice parameters given

in the publication, differing on average by one estimated standard deviation; the 28° C bond lengths and angles are particularly in error. For the analysis reported here, all bond lengths and angles were recalculated from the listed fractional coordinates and lattice parameters. The aristotype was defined from the 28° C data set, using the *z* fractional coordinate of 0.43895 and lattice parameter of 8.88696 Å. The crystal structure at each of the 14 temperatures was mode decomposed by the method detailed in the earlier section. As an example, the matrices, absolute coordinates, displacement vectors, mode amplitudes and phases, and bond lengths and angles for the 982° C crystal structure are listed in Table 5; observed (i.e. recalculated) bond lengths and angles shown in italics. The agreement between mode decomposition and calculation (observed) is excellent.

The temperature dependences of the six modes are illustrated in Figures 4a and b, and, as expected for a phase that is evolving in the absence of a structural phase transition, all are found to vary monotonically with temperature. Percentage changes in the mode amplitudes are -13.2, 63.1, 136.0, 10.9, 39.5, 216.8 for d1, d2, d3, d1′, d2′ and d3′ respectively. The most significant changes are associated with the modes that rotate the two tetrahedral sites relative to the aristotype orientation (d3, d3′). The percentage variation of the breathing modes (d1, d1′) are unsurprisingly much smaller and hence show no evidence for disordering of the two tetrahedral sites. The full lines on these figures show quartic polynomial fits to the mode data, noting that extrapolation beyond the range of the fits is inadvisable in such high-order polynomials (Hahn, 1977). The dashed lines on the identical figures show the mode expansivity ($\frac{1}{\mathrm{di}(')}\frac{d\mathrm{di}(')}{d\mathrm{T}}$), with the exception of d3′, as the magnitude of this mode passes through 0 at a temperature of T = ~82.18 °C. In this case, the mode expansivity is approximated by $\frac{1}{\mathrm{d3}'(500°\mathrm{C})}\frac{d\mathrm{d3}'}{d\mathrm{T}}$. Over the entire temperature interval, the mean mode expansion coefficients are -1.43×10^{-4} °C^{-1}, 8.21×10^{-4} °C^{-1}, 19.22×10^{-4} °C^{-1}, 1.20×10^{-4} °C^{-1}, 4.89×10^{-4} °C^{-1} and 28.01×10^{-4} °C^{-1} for d1, d2, d3, d1′, d2′ and d3′ respectively.

Using the polynomial parameterisation for the mode amplitudes and phases, and a quadratic fit to the lattice parameter variation with temperature, the derived structural parameters were calculated using the expressions shown earlier for the bond lengths/angles. The mode predicted variations are illustrated in Figures 5a, b and c as the full lines where they are compared with the observed results re-evaluated from the published fractional coordinates and lattice parameters. The agreement is excellent with the mode derived values less than 1 estimated standard deviation of the experimental values. The temperature invariance of the two T-site – O bond lengths is reproduced by mode decomposition; the apparent oscillatory behaviour of Al – O is within the scatter of the experimental results. Deducing a mechanism for the constant T-sites – O bond lengths with temperature, however, is not easy to determine as $\frac{1}{\mathrm{r}}\frac{d\mathrm{r}}{d\mathrm{T}} = \frac{\mathbf{r}}{\mathrm{r}^2}\bullet\frac{d\mathbf{r}}{d\mathrm{T}}$, and this algebraic expansion is unfortunately too unwieldy to derive the dominant terms for either case.

With the exception of the temperature variations of the bond lengths and angles, structural distortions of the two tetrahedral sites in sodalite were not considered in detail by Hassan et al. (2004). Re-analysis of their published data shows that the volumes of the tetrahedral sites reduce in a linear manner with increasing temperature as illustrated in Figure 6 where the volume of the AlO_4 tetrahedron varies as $(2.7105(1) - 9.6(2) \times 10^{-6}\ \mathrm{T})$ Å^3 (T °C) ($r^2 = 0.99375$), and the SiO_4 tetrahedron as $(2.1738(3) - 1.29(5) \times 10^{-5}\ \mathrm{T})$ Å^3 (T °C) ($r^2 = 0.97843$). The polyhedral distortion parameters of quadratic elongation (QE) and tetrahedral angle variance (TAV) (Robinson et al., 1971) are found to

vary linearly with temperature for both sites (QE Al - O = 1.00057 + 2.413 × 10^{-6} T (T °C), r^2 = 0.99336; QE Si - O = 1.00249 + 4.031 × 10^{-6} T, r^2 = 0.98836; TAV/degrees^2 AlO_4 = 2.2345 + 9.23 × 10^{-3} T, r^2 = 0.99327; TAV/degrees^2 SiO_4 = 9.6045 + 1.51 × 10^{-2} T, r^2 = 0.98788) but also vary monotonically with the corresponding value of the mode amplitudes that transform as the irreducible representation *E*, thus providing further evidence for this mode being related to the tetrahedral distortion. These variations with the *E* mode amplitude are shown in Figure 7 where the full and dashed lines are guides to the eye based on quadratic fits to the calculated distortion parameters. It should be noted that whilst the quadratic elongation and tetrahedral angle variance of the two T-sites are well separated as a function of temperature, the variation of the individual distortion parameter for both sites is almost continuous in the *E* mode amplitude. The lack of high temperature crystallographic results for other sodalite-structured phases precludes making any conclusion on whether this is typical or atypical behaviour.

Hassan et al. (2004) considered the structural basis for the thermal expansion of sodalite to be related to the temperature-induced weakening of the Na – Cl bonds. The migration of the Na ion towards the six-membered ring causes the tetrahedral sites to rotate relative to one another. Calculated bond valence sums (Brown, 2002) for the 7 coordinated NaO_6Cl site show it to be slightly under-bonded at room temperature, and significantly under-bonded at the highest temperatures measured. Manual adjustment of the R_0 values by allowing them to have a temperature dependence (R_0(T) = R_0(25 °C) + *c*T) (T °C) c ~ 9 × 10^{-3} pm °C^{-1} for Na – O, and c ~ 6 × 10^{-3} pm °C^{-1} for Na – Cl) gives a slightly over-bonded, but constant bond valence sum for all temperatures. However, RUM analysis (Hammonds, 1996; Dove et al., 2007) has found the SOD framework to be intrinsically flexible with zero-frequency modes throughout much of the Brillouin zone. It therefore seems more plausible that the thermal expansion of sodalite is governed by the behaviour of these low frequency rigid unit modes which permit the tetrahedra to rotate relative to one another with the Na moving towards the six-membered ring to maintain bond valency. Low frequency external modes (< 300 cm^{-1}) have been observed in the Raman spectrum of sodalite, with a single band measured as low as 59 cm^{-1}, compared to the "free TO_4" modes that lie in the range 350 - 1150 cm^{-1} (Arai and Smith, 1981).

Discussion and conclusions

Analysis of the anion fractional coordinates of the SOD framework for sodalite-structured phases in space group $P\bar{4}3n$ have shown that an aristotype phase can be derived for sets of fractional coordinates (x, x, z) for $x^2 - x - z^2 + z - 1/8 = 0$. The observed crystal structure of the SOD framework in sodalite-structured phases has been shown to parameterisable in terms of normal mode amplitudes of the ideal tetrahedral "molecule" for this aristotype crystal structure. Modes consistent with the point group symmetry of the two symmetry-independent T-sites in sodalite ($\bar{4}$) transform as the irreducible representations A_1, $E(\alpha)$ and T_1(z); a breathing mode, a tetrahedral distortion mode and a rigid body rotation. The methodology, demonstrated for a phase at a fixed thermodynamic state, is shown to be simply extended to variable thermodynamic conditions. Fitting the thermodynamic variation of the mode amplitudes to low order polynomial functions of the thermodynamic variable permit an accurate interpolation of the SOD framework at unmeasured values of the variable as illustrated in the analysis of high temperature sodalite data. Extrapolation of the polynomials beyond the fixed extrema of measured data is not to be recommended, however, it is possible that fitting mode amplitudes to sets of orthogonal polynomials rather than simple polynomials may permit some level of extrapolation.

The hierarchy of the SOD framework in space groups $Im\bar{3}m$, $I\bar{4}3m$, $Pm\bar{3}n$ and $P\bar{4}3n$, with one, two, two and three free anion fractional coordinates respectively, however, illustrates a surprising result with the mode analysis. The expectation that the crystallographic degrees of freedom would equal the number of active modes initially does not appear to hold. In the body-centred space group $Im\bar{3}m$ ($x + u$, $x + u$, 0.5) two modes are found (A_1 and E) with one free fractional coordinate, and in $I\bar{4}3m$ ($x + u$, $x + u$, 0.5 + w) three modes are found (A_1, E and T_1) with two free fractional coordinates. The disagreement between crystallographic and mode degrees of freedom is, however, only superficial, as analysis of the ratio of A_1/E mode amplitudes in the body-centred space groups shows them to be in a fixed ratio, for example setting the aristotype $z = 0.5$ this ratio is $(2 - \sqrt{2})/(1 + \sqrt{2})$ (~0.2426) thus reducing the mode degrees of freedom by one. For other choices of aristotype z, the ratio will be different, for example setting the aristotype $z = 0.4220$, the z fractional coordinate of the anion in bicchulite at room temperature (Sahl, 1980), the ratio is ~0.1430. In the primitive space groups the mode degrees of freedom matches the crystallographic degrees of freedom; $Pm\bar{3}n$ ($x + u$, $x + v$, 0.5) two independent mode amplitudes are found (A_1 and $E(\alpha)$) for two free anion fractional coordinates, $P\bar{4}3n$ ($x + u$, $x + v$, 0.5 + w) three independent modes are found (A_1, $E(\alpha)$ and $T_1(z)$) for three free anion fractional coordinates.

The general applicability of mode decomposition to characterise the SOD framework in other sodalite-structured, lower symmetry phases than those discussed here requires further detailed analysis. However, a simple global optimisation strategy shows that the ambient temperature crystal structure of tugtupite ($Na_4AlBeSi_4O_{12}Cl$) (Antao et al, 2004b) in space group $I\bar{4}$ is amenable to this analysis with regular tetrahedra found for the 3 T-sites (Be, Al, Si) at the expense of crystal-chemically implausible bond lengths. In this respect, this derived crystal structure is similar to that found for garnet (Knight, 2019) in that it is topologically consistent i.e. a prototypic crystal structure but not an aristotype crystal structure in the strict sense of Megaw (1973). Observed and optimised aristotype crystallographic parameters for tugtupite at 33 °C are listed in Table 6.

The belief that pure silica sodalite represents the highest symmetry SOD framework in space group $Im\bar{3}m$ (Richardson et al., 1988, Fischer and Bauer, 2009) requires comment since there are no differences in the systematic absence conditions for space groups $Im\bar{3}m$ and $I\bar{4}3m$. Table 1 shows that in space group $Im\bar{3}m$ the anion fractional coordinate is (x, x, 1/2) and in $I\bar{4}3m$ (x, x, z) (z ~ 1/2). The single crystal X-ray diffraction results found $z = 0.505$ (Richardson et al., 1988), however this fractional coordinate was set to zero despite an estimated standard deviation of 0.001 i.e. five standard deviations from zero. Justification for setting the fractional coordinate to zero was not given in the work of Richardson et al. (1988) and confirmation of their choice of space group is required. Providing data were collected at a suitable X-ray wavelength to excite anomalous scattering from silicon, the point group symmetry of a large volume of reciprocal space should provide evidence for the correct space group of pure silica sodalite due to the breakdown of Friedel's/Bijvoet's law. Despite the low atomic number of silicon, and hence the expectation that anomalous scattering effects will be small, Lang (1965) has shown however, that imaging of Brazil twins in quartz is possible using Co $K\alpha$ or Cu $K\alpha$ radiation due to strong anomalous dispersion associated with certain reflections.

The lack of a unique set of anion fractional coordinates for the aristotype phase for the sodalite structure probably renders distance least squares modelling unreliable to predict the evolution of the crystal structure when the input data is purely based on lattice parameter data. It is close to

twenty years since sodalite has been studied crystallographically at high temperature and it would be timely to remeasure again, including a structural investigation of the bromine and iodine analogues in addition. The ease of bulk synthesis of sodalite (Stein et al., 1992) would permit samples suitable for neutron powder diffraction to be produced. Al and Si can be easily distinguished using neutron diffraction due to significantly different scattering lengths, whereas Si^{4+} and Al^{3+} are to first order isoelectronic form factors for X-ray diffraction. The use of time-of-flight neutron powder diffraction with simultaneous high-Q and low-Q coverage would allow any site occupancy variation at the T-sites as a function of temperature to be decorrelated from the atomic displacement parameters, should any site disordering occur. Structural results from $Na_8[Si_6Al_6O_{24}]I_2$ could then be compared with the results of distance least squares modelling (Dempsey and Taylor, 1980) to investigate the validity of the method for this particular structure type.

The measurement of Cl-, Br-, I-sodalite as a function of temperature coupled with mode analysis may shed more light on the mechanisms underlying the thermal expansion behaviour of these materials.

Acknowledgements

Prof. A. G. Christy (University of Queensland) and Prof. S. E. Dann (Loughborough) are thanked for constructive reviews, and Dr. Stuart Mills is thanked for editorial handling of the submission. I am grateful to Dr. Richard Jones (Keele) for reading and commenting on an early draft of the manuscript, and to Prof. Sandie Dann for the reference to Fischer and Bauer. This work is dedicated to my friends and collaborators of 30 years, Dr. Richard Hywel Jones and Prof. Christopher Michael Bradford "Mike" Henderson, in recognition of their important contributions to the structural chemistry of microporous solids (Jones) and aluminosilicates (Henderson).

584 **References**

585 Antao S.M. (2021) Linear structural trends and multi-phase intergrowths in helvine-group minerals,
586 $(Zn,Fe,Mn)_8[Be_6Si_6O_{24}]S_2$. *Minerals*, **11**, 325-346.

587 Antao S.M., Hassan I and Parise J.B. (2003) The structure of danalite at high temperature obtained
588 from synchrotron radiation and Rietveld refinement. *The Canadian Mineralogist*, **41**, 1413-1422.

589 Antao S.M., Hassan I. and Parise J.B. (2004a) Chromate aluminate sodalite $Ca_8[Al_{12}O_{24}](CrO_4)_2$:
590 Phase transitions and high-temperature structural evolution of the cubic phase. *The Canadian*
591 *Mineralogist*, **42**, 1047-1056.

592 Antao S.M., Hassan I. and Parise J.B. (2004b) Tugtupite: High temperature structures obtained from
593 in situ synchrotron diffraction and Rietveld refinement. *American Mineralogist*, **89**, 492-497.

594 Arai J. and Smith S.R.P. (1981) The Raman spectrum and analysis of phonon modes in sodalite.
595 *Journal of Physics C*: *Solid State Physics*, **14**, 1193-1202.

596 Aroyo M.I., Kirov A., Capillas C., Perez-Mato J.M. and Wondratschek H. (2006) Bilbao
597 Crystallographic Server II: Representations of crystallographic point groups and space groups. *Acta*
598 *Crystallographica*, A**62**, 115-128.

599 Bärnighausen H. (1975) Group-subgroup relationships between space groups as an ordering principle
600 in crystal-chemistry – Family tree of perovskite-like structures. *Acta Crystallographica*, A**31**, S3.

601 Barth T.H.F. (1926) Die kristallographische Beziehung zwischen Helvin und Sodalit. *Norsk*
602 *Geologisk Tidsskrift*, **9**, 40-42.

603 Beagley B., Henderson C.M.B. and Taylor D. (1982) The crystal structures of aluminosilicate-
604 sodalites: X-ray diffraction studies and computer modelling. *Mineralogical Magazine*, **46**, 459-464.

605 Bishop D.M. (1972) *Group Theory and Chemistry*. Clarendon Press, Oxford, 300p.

606 Bradley C.J. and Cracknell A.P. (1972) *The Mathematical Theory of Symmetry in Solids*. Clarendon
607 Press, Oxford, 745 p.

608 Brown I.D. (2002) *IUCr Monographs on Crystallography 12. The Chemical Bond in Inorganic*
609 *Chemistry.* International Union of Crystallography, Oxford, 278 p.

610 Buerger M.J. (1947) Derivative crystal structures. *Journal of Chemical Physics*, **15**, 1-16.

611 Buerger M.J. (1961) Polymorphism and phase transitions. *Fortschritte der Mineralogie,*
612 *Kristallographie und Petrologie*, **39**, 9-24.

613 Decius J.C. and Hexter R.M. (1977) *Molecular Vibrations in Crystals*. McGraw-Hill, New York,
614 391p.

615 Deer W.A., Howie R.A., Wise W.S. and Zussman J. (2004) *Rock Forming Minerals, Volume 4B,*
616 *Framework Silicates: Silica Minerals, Feldspathoids and the Zeolites*, The Geological Society,
617 London, 982 p.

618 Dempsey M.J. and Taylor D. (1980) Distance least squares modelling of the cubic sodalite structure
619 and of the thermal expansion of $Na_8(Al_6Si_6O_{24})I_2$. *Physics and Chemistry of Minerals*, **6**, 197-208.

Dove M.T., Pryde A.K.A., Heine V. and Hammonds K.D. (2007) Exotic distributions of rigid unit modes in the reciprocal spaces of framework aluminosilicates. *Journal of Physics: Condensed Matter*, **19**, 275209.

El-Betanouny M. and Wooten F. (2008) *Symmetry and Condensed Matter Physics*. Cambridge University Press, Cambridge, 922 p.

Fischer R.X. and Bauer W.H. (2009) Symmetry relationships of sodalite (SOD) – type crystal structures. *Zeitschrift für Kristallographie*, **224**, 185-197.

Gottfried C. (1927) Die Raumgruppe des Helvins. *Zeitschrift für Kristallographie*, **65**, 425-427.

Hahn G.J. (1977) The hazards of extrapolation in regression analysis. *Journal of Quality Technology*, **9**, 159-165.

Hammonds K.D., Dove M.T., Giddy A.P., Heine V. and Winkler B. (1996) Rigid-unit phonon modes and structural phase transitions in framework silicates. *American Mineralogist*, **81**, 1057-1079.

Hassan I., Antao S.M. and Parise J.B. (2004) Sodalite: High-temperature structures obtained from synchrotron radiation and Rietveld refinements. *American Mineralogist*, **89**, 359-364.

Hassan I and Grundy H.D. (1984) The crystal structure of sodalite-group minerals. *Acta Crystallographica*, B**40**, 6-13.

Hassan I and Grundy H.D. (1985) The crystal structures of the helvite-group minerals, $(Mn,Fe,Zn)_8[Be_6Si_6O_{24}]S_2$. *American Mineralogist*, **70**, 186-192.

Howard C.J. and Stokes H.T. (2004) Structures and phase transitions in perovskites: a group-theoretical approach. *Acta Crystallographica*, A**61**, 93-111.

Jaeger F.M. (1929) On the constitution and structure of ultramarine. *Transactions of the Faraday Society*, **25**, 320-345.

Jaeger F.M., Westenbrin H.G.K. and van Mellf F.A. (1927) Roentgenspectrographic investigations on the structure of the artificial ultramarines and the problem concerning their relations to the minerals hauyne nosean sodalite lazurite and nephelite. *Proceedings of the Koninklijke Akademie van Wetenschappen te Amsterdam*, **30**, 249-267.

King R.S.P., Dann S.E., Elsegood M.R.J., Kelly P.F. and Mortimer R.J. (2009) The synthesis, full characterisation and utilisation of template-free silica sodalite, a novel polymorph of silica. *Chemistry, A European Journal*, **15**, 5441-5443.

Knight K.S. (2019) Parameterization of the crystal structure of garnet in terms of symmetry-adapted basis-vectors of the ideal tetrahedron and octahedron: Application to the pressure-dependence of the crystal structure of $Y_3Al_5O_{12}$ between 0 and 126 GPa. *Materials Chemistry and Physics*, **227**, 72-82.

Knight K.S. and Henderson C.M.B. (2019) Defining an aristotype crystal structure and crystallographic distortions in leucite/pollucite-structured phases with space group $Ia\bar{3}d$. *Physics and Chemistry of Minerals*, **46**, 595-605.

Kudoh Y. and Takéuchi Y. (1985) The effect of pressure on helvite $Mn_8S_2[Be_6Si_6O_{24}]$. *Zeitschrift für Kristallographie*, **173**, 305-312.

Ladd M. (2014) *Symmetry of Crystals and Molecules*. Oxford University Press, Oxford, 464 p.

Lang A.R. (1965) Mapping Dauphiné and Brazil twins in quartz using X-ray topography. *Applied Physics Letters*, 7, 168-170.

Löns J. and Schulz H. (1967) Strukturverfeinerung von Sodalith, $Na_8Si_6Al_6O_{24}Cl_2$. *Acta Crystallographica*, B**52**, 616-627.

Loewenstein W. (1954) The distribution of aluminium in the tetrahedra of silicates and aluminates. *American Mineralogist*, **39**, 92-96.

McMullan R.K., Ghose S., Haga N. and Schomaker V. (1996) Sodalite, $Na_4Si_3Al_3O_{12}Cl$: Structure and ionic mobility at high temperatures by neutron diffraction. *Acta Crystallographica*, B**52**, 616-627.

Megaw H.D. (1973) *Crystal Structures. A Working Approach*. Saunders, London, 563p.

Meier W.M. and Villiger H. (1969) Die Methode der Abstandverfeinerung zur Bestimmung der Atomkoordinaten idealisierter Gerüststrukturen. *Zeitschrift für Kristallographie*, **129**, 411-423.

Müller U. (2013) *IUCr Texts on Crystallography 18. Symmetry Relationships Between Crystal Structures. Applications of Crystallographic Group Theory in Crystal Chemistry*, International Union of Crystallography, Oxford, 332 p.

O'Keeffe M. and Hyde B.G. (1996) *Mineralogical Society of America Monograph, Crystal Structures I. Patterns and Symmetry*, Mineralogical Society of America, Washington, 453p.

Pauling L. (1930) XXII. The structure of sodalite and helvite. *Zeitschrift für Kristallographie*, **74**, 213-225.

Poole D. (2014) *Linear Algebra: A Modern Introduction*. Cengage Learning, 720 p.

Richardson J.W., Pluth J.J., Smith J.V., Dytrych W.J. and Bibby D.M. (1988) Conformation of Ethylene Glycol and Phase Change in Silica Sodalite. *Journal of Physical Chemistry*, **92**, 243-247.

Robinson K., Gibbs G.V. and Ribbe P.H. (1971) Quadratic elongation: A quantitative measure of distortion in coordination polyhedral. *Science*, **172**, 567-570.

Sahl K. (1980) Refinement of the crystal structure of bicchulite $Ca_2[Al_2SiO_6](OH)_2$. *Zeitschrift für Kristallographie*, **152**, 13-21.

Smith J.V. (1982) *Geometrical and Structural Crystallography*, John Wiley & Sons, New York, 450 p.

Stein A., Ozin G.A., Macdonald P.M., Stucky G.D. and Jelinek R. (1992) Silver, sodium halosodalites: Class A sodalites. *Journal of the American Chemical Society*, **114**, 5171-5186.

Stokes H.T. and Hatch D.M. (1988) *Isotropy Subgroups of the 230 Crystallographic Space Groups*. World Scientific, Singapore, 624 p.

Taylor D. (1968) The thermal expansion of the sodalite group of minerals. *Mineralogical Magazine*, **36**, 761-769.

691 Taylor D. (1972) The thermal expansion behaviour of the framework silicates. *Mineralogical*
692 *Magazine*, **38**, 593-604.

693 Taylor D. (1975) Cell parameter correlations in the aluminosilicate-sodalites. *Contributions to*
694 *Mineralogy and Petrology*, **51**, 39-47.

695 Taylor D. (1983) The structural behaviour of tetrahedral framework compounds – a review. Part I.
696 Structural behaviour, *Mineralogical Magazine*, **47**, 319-326.

697 Taylor D. (1984) The structural behaviour of tetrahedral framework compounds – a review. Part II.
698 Framework structures. *Mineralogical Magazine*, **48**, 65-79.

699 Taylor D. and Henderson C.M.B. (1978) A computer model for the cubic sodalite structure. *Physics*
700 *and Chemistry of Minerals*, **2**, 325-336.

Table 1. Fractional coordinates for the T-sites and coordinating anions of the SOD framework in space groups $Im\bar{3}m$, $I\bar{4}3m$, $P\bar{4}3n$ and $Pm\bar{3}n$.

Space group	T-site	Anion site	Coordinating anions	
$Im\bar{3}m$	12*d* 1/4, 0, 1/2	24*h* *x*, *x*, 1/2	O1	*x*, *x*, 1/2
	$\bar{4}$m2	*x* ~ 0.14	O2	*x*, -*x*, 1/2
			O3	1/2-*x*, 0, 1/2-*x*
			O4	1/2-*x*, 0, 1/2+*x*
$I\bar{4}3m$	12*d* 1/4, 0, 1/2	24*h* *x*, *x*, *z*	O1	*x*, *x*, *z*
	$\bar{4}$	*x* ~ 0.14	O2	*x*, -*x*, 1-*z*
		z ~ 0.44	O3	1/2-*x*, -1/2+*z*, 1/2-*x*
			O4	1/2-*x*, 1/2-*z*, 1/2+*x*
$P\bar{4}3n$	6*d* 1/4, 0, 1/2	24*i* *x*, *y*, *z*	O1	*x*, *y*, *z*
	$\bar{4}$	*x* ~ *y* ~ 0.14	O2	*x*, -*y*, 1-*z*
		z ~ 0.44	O3	1/2-*x*, -1/2+*z*, 1/2-*y*
			O4	1/2-*x*, 1/2-*z*, 1/2+*y*
	6*c* 1/2, 0, 3/4		O4	1/2-*x*, 1/2-*z*, 1/2+*y*
	$\bar{4}$		O6	1/2+*x*, -1/2+*z*, 1/2+*y*
			O7	1-*z*, *x*, 1-*y*
			O8	*z*, -*x*, 1-*y*
$Pm\bar{3}n$	6*c* 1/4, 0, 1/2	24*k* *x*, *y*, 1/2	O1	*x*, *y*, 1/2
	$\bar{4}$m2	*x* ~ *y* ~ 0.14	O2	*x*, -*y*, 1/2
			O3	1/2-*x*, 0, 1/2-*y*
			O4	1/2-*x*, 0, 1/2+*y*
	6*d* 1/2, 0, 3/4		O4	1/2-*x*, 0, 1/2+*y*
	$\bar{4}$m2		O6	1/2+*x*, 0, 1/2+*y*
			O7	1/2, *x*, 1-*y*
			O8	1/2, -*x*, 1-*y*

706 **Table 2.** Symmetry-adapted basis-vector displacements for modes of point group $\bar{4}3m$ that are
707 consistent with point group $\bar{4}m2$ (A_1, $E(\alpha)$) and $\bar{4}$ (A_1, $E(\alpha)$, $T_1(z)$).

Irreducible representation	Displacement		
	i	**j**	**k**
A_1			
O1	$-d_1$	$-d_1$	d_1
O2	d_1	d_1	d_1
O3	d_1	$-d_1$	$-d_1$
O4	$-d_1$	d_1	$-d_1$
$E(\alpha)$			
O1	$-d_2$	$-d_2$	$-2d_2$
O2	d_2	d_2	$-2d_2$
O3	d_2	$-d_2$	$2d_2$
O4	$-d_2$	d_2	$2d_2$
$T_1(z)$			
O1	d_3	$-d_3$	0
O2	$-d_3$	d_3	0
O3	d_3	d_3	0
O4	$-d_3$	$-d_3$	0

708

709 **Table 3.** Absolute coordinates for the 6*c*, 6*d* tetrahedral sites in sodalite (T-sites at the origin).

	6*d* (**i**, **j**, **k** basis)		
O1	-*x* - d1 - d2 + d3 -*x* - d1 - d2 - d3 *x* + d1 - 2d2	O2	*x* + d1 + d2 - d3 *x* + d1 + d2 + d3 *x* + d1 - 2d2
O3	*x* + d1 + d2 + d3 -*x* - d1 - d2 + d3 -*x* - d1 + 2d2	O4	-*x* - d1 - d2 - d3 *x* + d1 + d2 - d3 -*x* - d1 + 2d2
	6*c* (**i′**, **j′**, **k′** basis)		
O4	-*x* - d1′ - d2′ + d3′ -*x* - d1′ - d2′ - d3′ *x* + d1′ - 2d2′	O6	*x* + d1′ + d2′ - d3′ *x* + d1′ + d2′ + d3′ *x* + d1′ - 2d2′
O7	*x* + d1′ + d2′+ d3′ -*x* - d1′ - d2′ + d3′ -*x* - d1′ + 2d2′	O8	-*x* - d1′ - d2′ - d3′ *x* + d1′ + d2′ - d3′ -*x* - d1′ + 2d2′

710 $x = a(-0.25 + (0.375 - z + z^2)^{0.5})$

711

712

713 **Table 4.** Comparison of derived structural parameters for sodalite based on crystal structure
714 refinement and mode decomposition.

	Hassan and Grundy (1984)	Mode decomposition
Al - O/Å	1.742	1.7416
O - Al - O/degrees (mult. 2)	111.0	111.04
O - Al - O/degrees (mult. 4)	108.7	108.69
Si - O/Å	1.620	1.6196
O - Si - O/degrees (mult. 2)	113.0	113.03
O - Si - O/degrees (mult. 4)	107.7	107.72
Al - O - Si/degrees	138.2	138.19

715

716

Table 5. Details of mode decomposition for the crystal structure of sodalite at 982 °C (Hassan et al., 2004). Bond lengths and angles recalculated from the published lattice parameter and fractional coordinates are shown in italics.

6*d*	**i**, **j**, **k** basis	6*c*	**i′**, **j′**, **k′** basis
M1	$\begin{pmatrix} 0 & -\alpha & \beta \\ 0 & \beta & -\alpha \\ -1 & 0 & 0 \end{pmatrix}$	**M2**	$\begin{pmatrix} \alpha & -\beta & 0 \\ -\beta & -\alpha & 0 \\ 0 & 0 & -1 \end{pmatrix}$
R	$\begin{pmatrix} \frac{1}{\sqrt{2}} & \frac{-1}{\sqrt{2}} & 0 \\ \frac{1}{\sqrt{2}} & \frac{1}{\sqrt{2}} & 0 \\ 0 & 0 & 1 \end{pmatrix}$	**R**	$\begin{pmatrix} \frac{1}{\sqrt{2}} & \frac{-1}{\sqrt{2}} & 0 \\ \frac{1}{\sqrt{2}} & \frac{1}{\sqrt{2}} & 0 \\ 0 & 0 & 1 \end{pmatrix}$
O1 aristotype/Å	$\begin{pmatrix} -0.96677 \\ -0.96677 \\ 0.96677 \end{pmatrix}$	O4 aristotype/Å	$\begin{pmatrix} -0.96677 \\ -0.96677 \\ 0.96677 \end{pmatrix}$
O1 hettotype/Å	$\begin{pmatrix} -1.14188 \\ -0.90848 \\ 0.95150 \end{pmatrix}$	O4 hettotype/Å	$\begin{pmatrix} -1.05737 \\ -0.87499 \\ 0.86059 \end{pmatrix}$
ΔO1/Å	$\begin{pmatrix} -0.17511 \\ 0.05829 \\ -0.01527 \end{pmatrix}$	ΔO4/Å	$\begin{pmatrix} -0.09060 \\ 0.09178 \\ -0.10618 \end{pmatrix}$
d1/Å	0.03385	d1′/Å	-0.03579
d2/Å	0.02456	d2′/Å	0.035200
d3/Å	-0.11670	d3′/Å	-0.09119
Al - O/Å	1.74200, *1.74201*	Si - O/Å	1.61995, *1.61998*
O – Al – O/degrees (2)	113.785, *113.788*	O – Si – O/degrees (2)	115.821, *115.823*
O – Al – O/degrees (4)	107.358, *107.357*	O – Si – O/degrees (4)	106.393,*106.392*
Si – O - Al	143.349, *143.347*		

$\alpha = 0.917894$, $\beta = 0.396825$, $a_a = 8.88696$ Å, $z = 0.43895$

722 **Table 6.** Comparison of the observed fractional coordinates in tugtupite at room temperature (Antao
723 et al., 2004b) with an aristotype with ideal tetrahedral geometry at the three symmetry-independent T-
724 sites.

		Observed structural parameters	Optimised aristotype structural parameters
Si (8*g*)	*x*	0.7461	0.76531
	y	0.0133	0.01675
	z	0.5051	0.50229
O1 (8*g*)	*x*	0.1051	0.14403
	y	0.1367	0.12393
	z	0.4433	0.45296
O2 (8*g*)	*x*	0.1562	0.16452
	y	0.4641	0.47504
	z	0.1503	0.13540
O3 (8*g*)	*x*	0.4249	0.42813
	y	0.1430	0.16470
	z	0.1391	0.12624
Be - O2/Å		1.640	1.7580
Al - $O3^{i}$/Å		1.705	1.8984
Si - $O2^{iii}$/Å		1.560	1.5083
Si - $O1^{i}$/Å		1.620	1.5083
Si - $O3^{iv}$/Å		1.645	1.5083
Si - $O1^{ii}$/Å		1.666	1.5083
O2 - Be - $O2^{i}$/° ×4		106.84	109.471
O2 - Be - $O2^{ii}$/° ×2		114.87	109.471
$O3^{i}$ - Al - $O3^{ii}$/° ×4		109.39	109.471
$O3^{i}$ - Al - $O3^{iii}$/° ×2		109.64	109.471
$O1^{i}$ - Si - $O2^{iii}$/°		106.01	109.471
$O2^{iii}$ - Si - $O3^{iv}$/°		117.34	109.471
$O1^{i}$ - Si - $O2^{iii}$/°		109.06	109.471
$O1^{i}$ - Si - $O3^{iv}$/°		108.69	109.471
$O1^{i}$ - Si - $O1^{ii}$/°		108.85	109.471
$O1^{ii}$ - Si - $O3^{iv}$/°		106.69	109.471

725 Space group: $I\bar{4}$, a = 8.62597 Å, c = 8.8564 Å

726 Al (2*d*): 0.00, 0.50, 0.75, Be (2*c*): 0.00, 0.50, 0.25

727 $O1^{i}$: 1 - *y*, *x*, 1 - *z*; $O1^{ii}$: 1 - *x*, -*y*, *z*

728 $O2^{i}$: -*x*, 1 - *y*, *z*; $O2^{ii}$: 1/2 - *y*, 1/2 + *x*, 1/2 - *z*; $O2^{iii}$: 1/2 + *x*, -1/2 + *y*, 1/2 + *z*

729 $O3^{i}$: *y*, 1 - *x*, 1 - *z*; $O3^{ii}$: -1/2 + *x*, 1/2 + *y*, 1/2 + *z*; $O3^{iii}$: -*y*, *x*, 1 - *z*; $O3^{iv}$: 1/2 + *y*, 1/2 - *x*, 1/2 - *z*

730

Figure Captions

Fig. 1

The crystal structure of sodalite at room temperature and pressure (Hassan and Grundy, 1984) viewed down [010] with [100] vertical. SiO_4 tetrahedra are shown as crosses, AlO_4 tetrahedra as orthogonal lines. Sodium cations are illustrated as plain circles, chlorine anions as straight lines and oxygen atoms as orthogonal lines.

Fig. 2

2a: The aristotype SOD topology in space group $Im\bar{3}m$ with undifferentiated T-site (12 *d*) and the direction of the $\bar{4}$ axis shown as an arrow.

2b: The structural topology of the hettotype phase in space group $Pm\bar{3}n$ with differentiated T-sites (6 *c* and 6 *d*). The directions of the two $\bar{4}$ axes from the symmetry independent tetrahedra are shown as arrows.

2c: The structural topology of the hettotype phase in space group $I\bar{4}3m$ with undifferentiated T-site (12 *d*) and the direction of the $\bar{4}$ axis shown as an arrow.

2d: The structural topology of the hettotype phase in space group $P\bar{4}3n$ (the sodalite structure) with differentiated T-sites (6 *c* and 6 *d*). The directions of the two $\bar{4}$ axes from the symmetry independent tetrahedra are shown as arrows.

For atom labelling see Table 1. The active irreducible representations relating two crystal structures are shown in Miller-Love notation (Stokes and Hatch, 1988) and designated by an arrow.

Fig. 3

Symmetry adapted basis vectors of the isolated TO_4 group consistent with point group symmetry $\bar{4}$. Upper left shows the orthonormal basis vectors used in the mode parameterisation with **k** perpendicular to the page. A_1 is a breathing mode with displacement amplitude d1(′), $E(\alpha)$ a tetrahedral distortion mode with displacement amplitude d2(′), and $T_1(z)$ is a rigid body rotation around **k** for small basis vector displacements d3(′).

Fig. 4

The temperature dependence of the mode displacement amplitudes and phases of the SOD framework of sodalite at high temperature derived from the crystallographic results of Hassan et al. (2004). Figure 4a illustrates the modes in the AlO_4 tetrahedron, Figure 4b the modes in the SiO_4 tetrahedron. In both cases, the calculated mode amplitudes are shown as circles, with the full lines on the figure showing quartic fits to these data. The mode expansion coefficients are shown as the dashed lines on the figure.

766

767 **Fig. 5**

768 Comparison of the observed, derived structural parameters of sodalite at high temperature (Hassan et
769 al., 2004) (shown as circles) with those calculated by mode decomposition (as the full lines). In all
770 cases the bond lengths and angles were recalculated from the published lattice parameters and
771 fractional coordinates as the tabulated data were inconsistent with these results. Figure 5a shows the
772 results from the AlO_4 tetrahedron, Figure 5b the results from the SiO_4 tetrahedron, whilst Figure 5c
773 shows the intra-polyhedral rotation angle. The agreement between the observed data and the
774 temperature variation calculated by mode parameterisation is excellent for all temperatures indicating
775 the ability for mode decomposition to accurately interpolate the structural parameters at intermediate
776 temperatures.

777

778 **Fig. 6**

779 The linear temperature dependences of the tetrahedral volumes of the AlO_4 and SiO_4 tetrahedra in
780 sodalite.

781

782 **Fig. 7**

783 The correlation of the structural distortion parameters of quadratic elongation and tetrahedral angle
784 variance (Robinson et al., 1971) with the amplitudes of the $E(\alpha)$ normal modes in sodalite at high
785 temperatures (Hassan et al., 2004). Despite the magnitudes of the quadratic elongation and tetrahedral
786 angle variance of the two tetrahedra being well separated in temperature, they follow identical trends
787 in the $E(\alpha)$ normal mode amplitudes. Further work is necessary to determine whether this is a
788 common structural response of sodalite-structured phases.

789

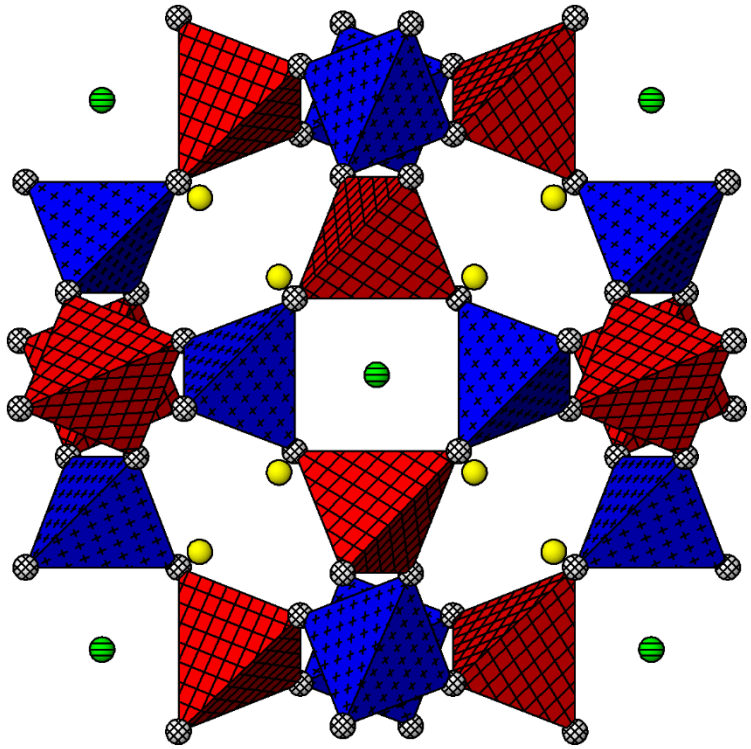

790

791 Figure 1

792

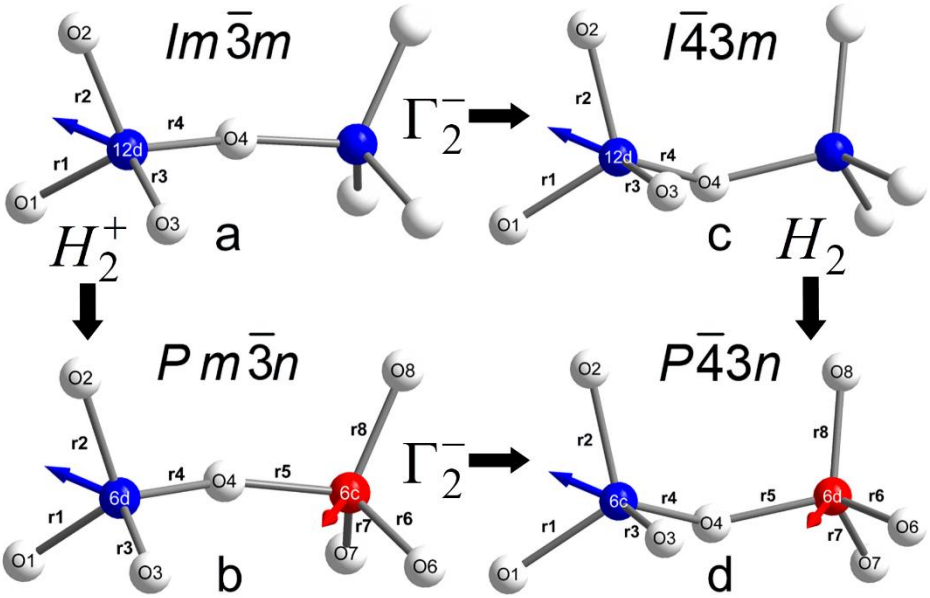

793

794 Figure 2

795

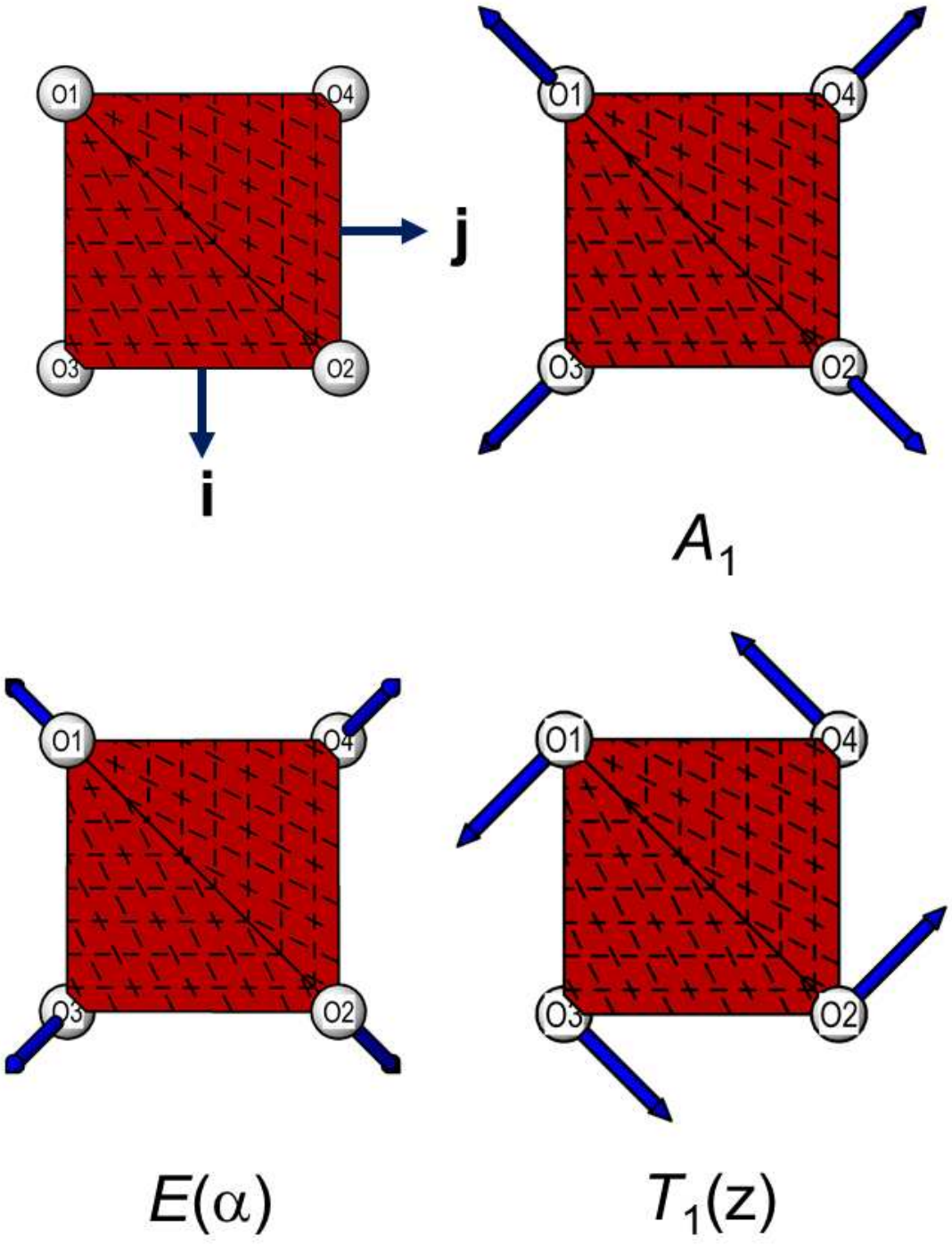

796

797 Figure 3

798

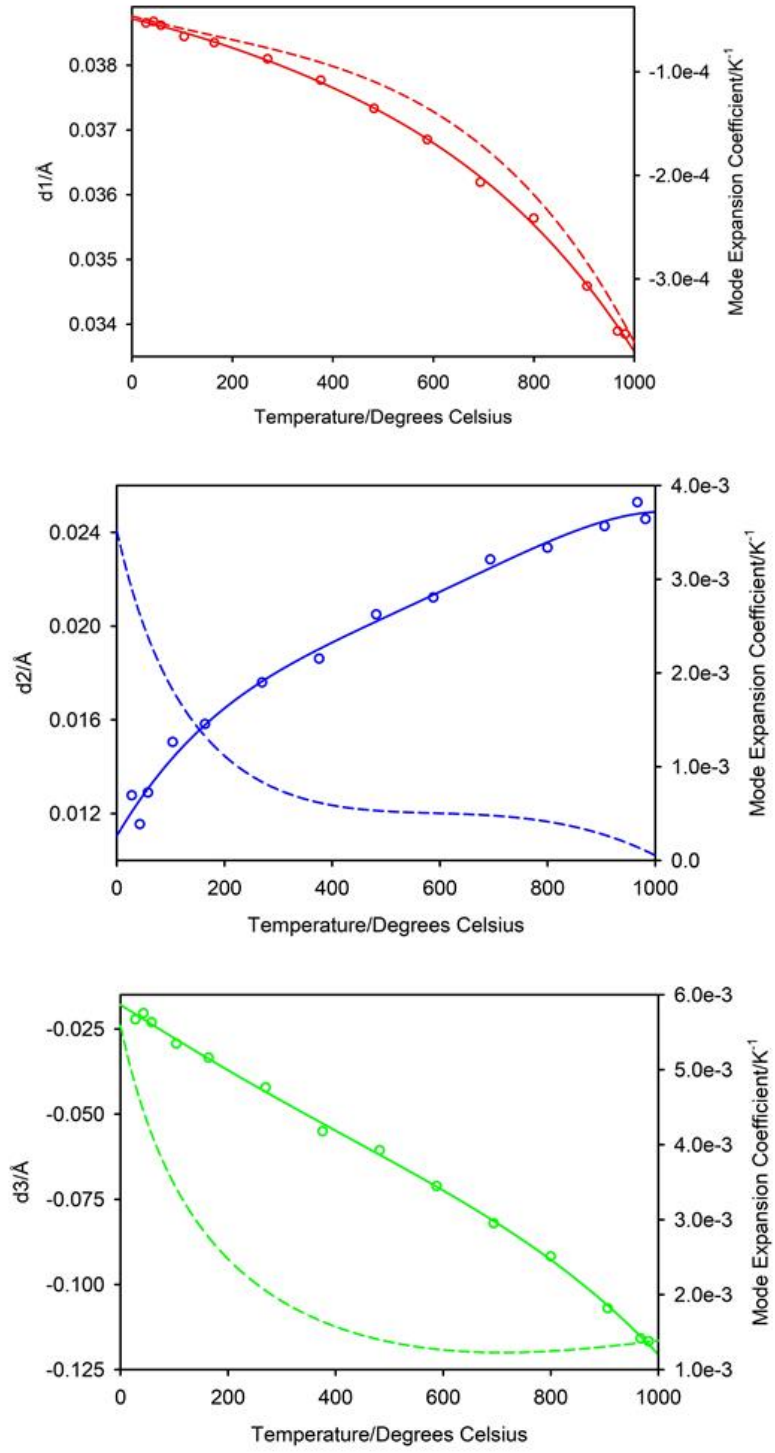

799

800 Figure 4a

801

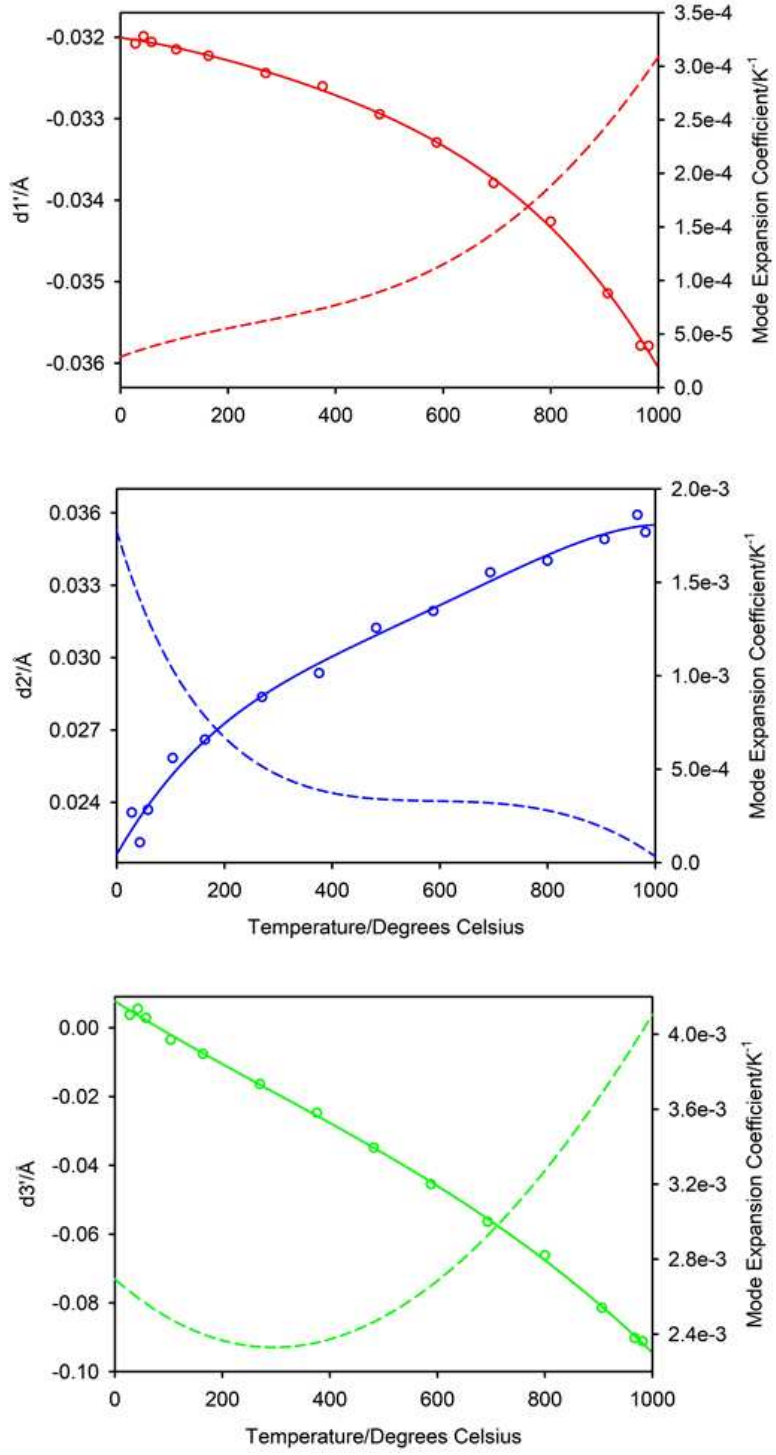

802

803 Figure 4b

804

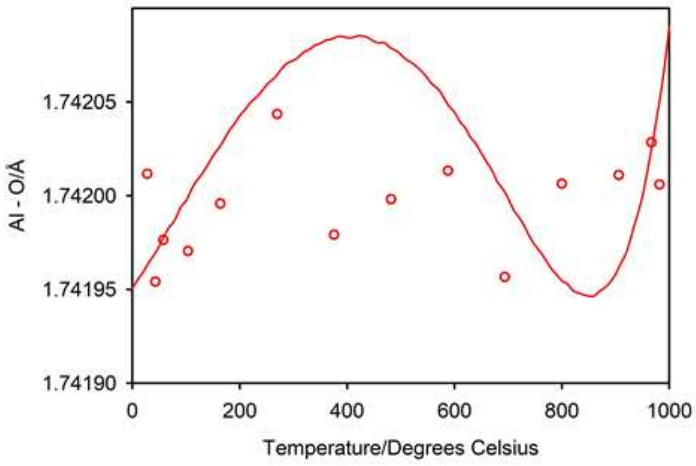

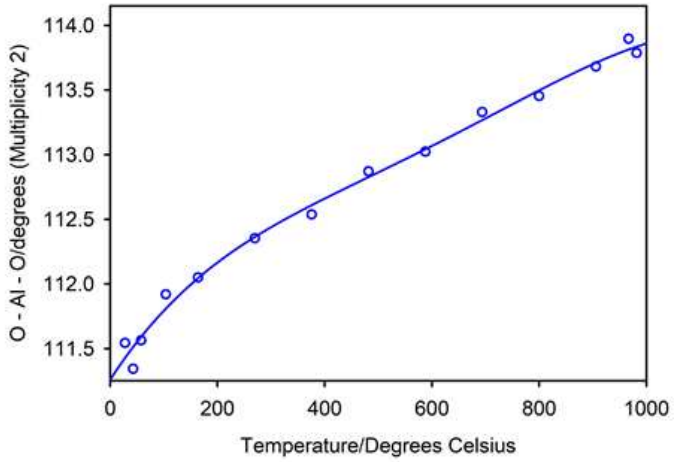

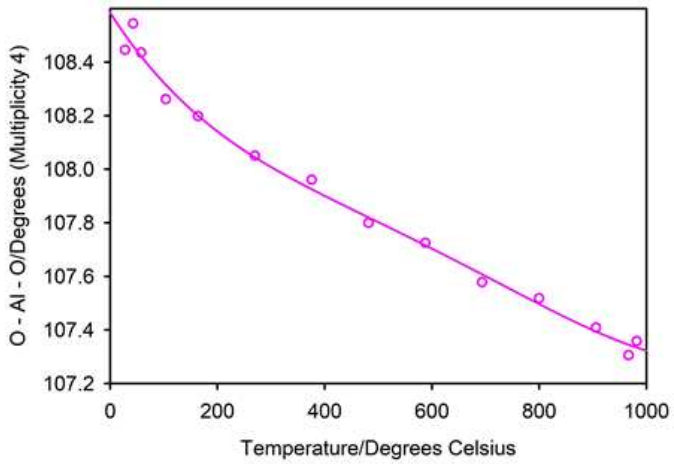

805

806 Figure 5a

807

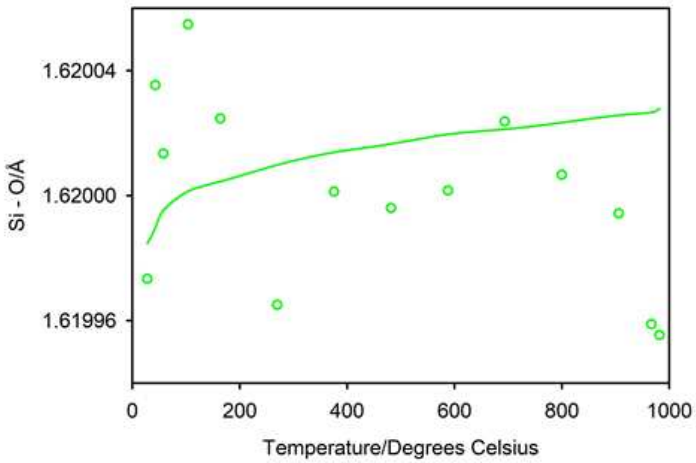

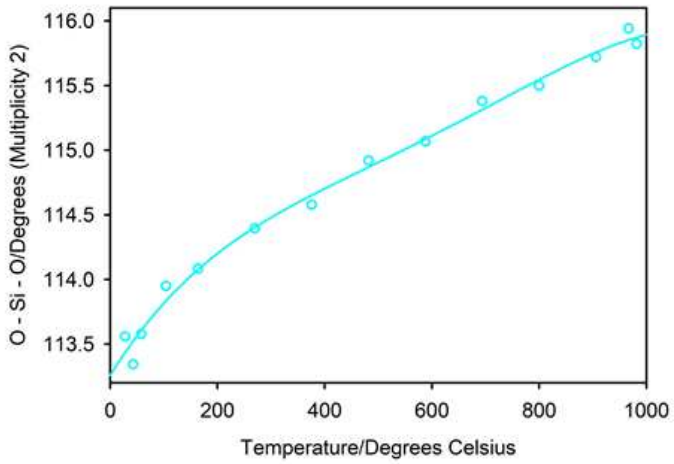

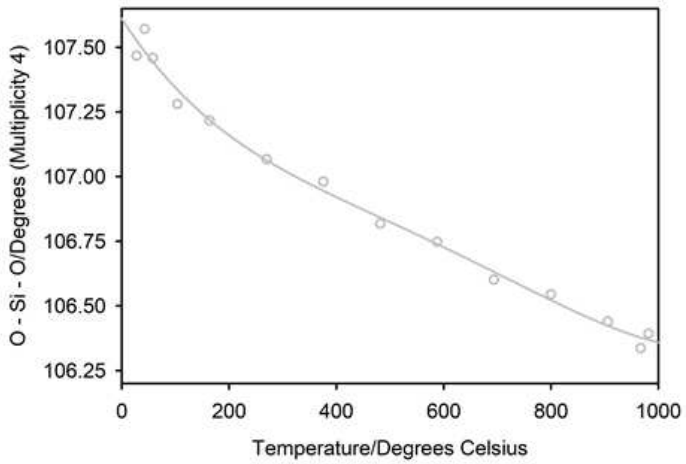

808

809 Figure 5b

810

811

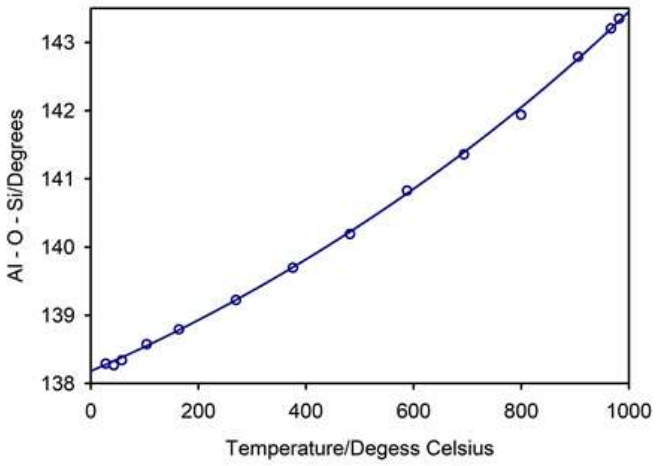

812

813 Figure 5c

814

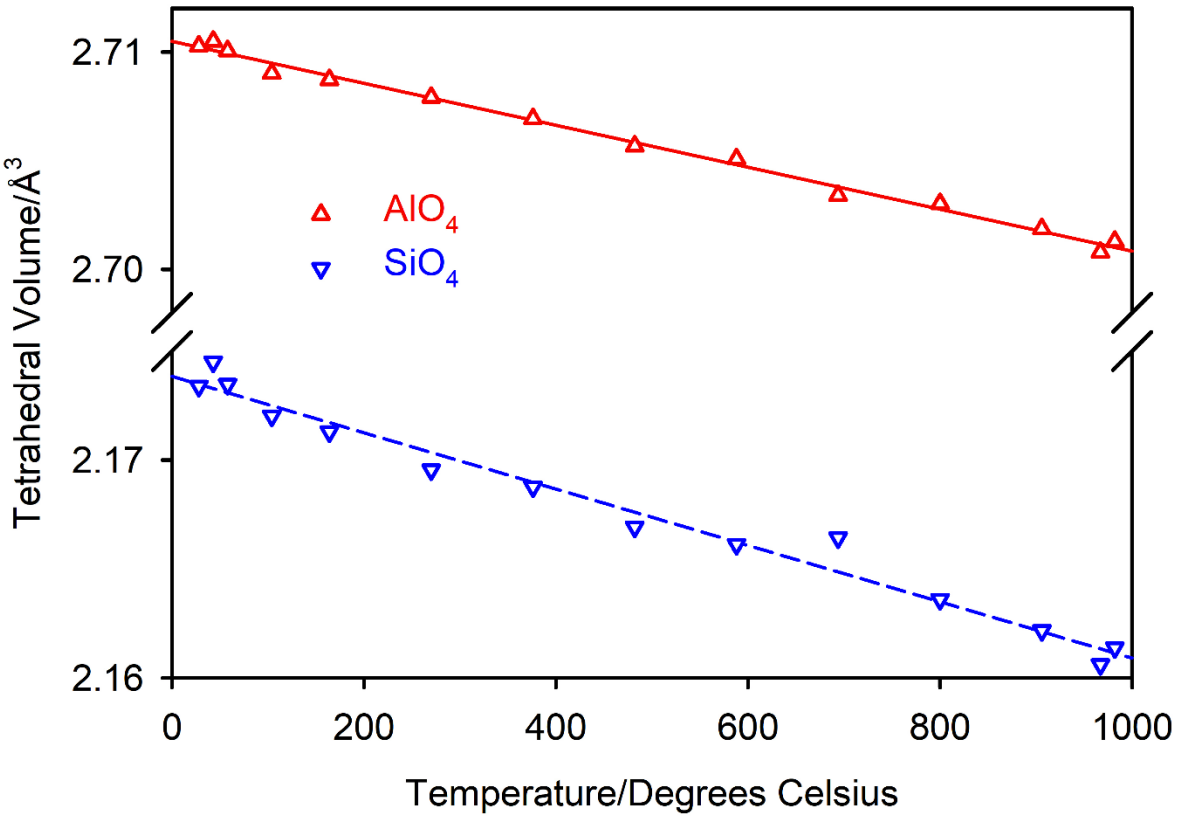

815

816 Figure 6

817

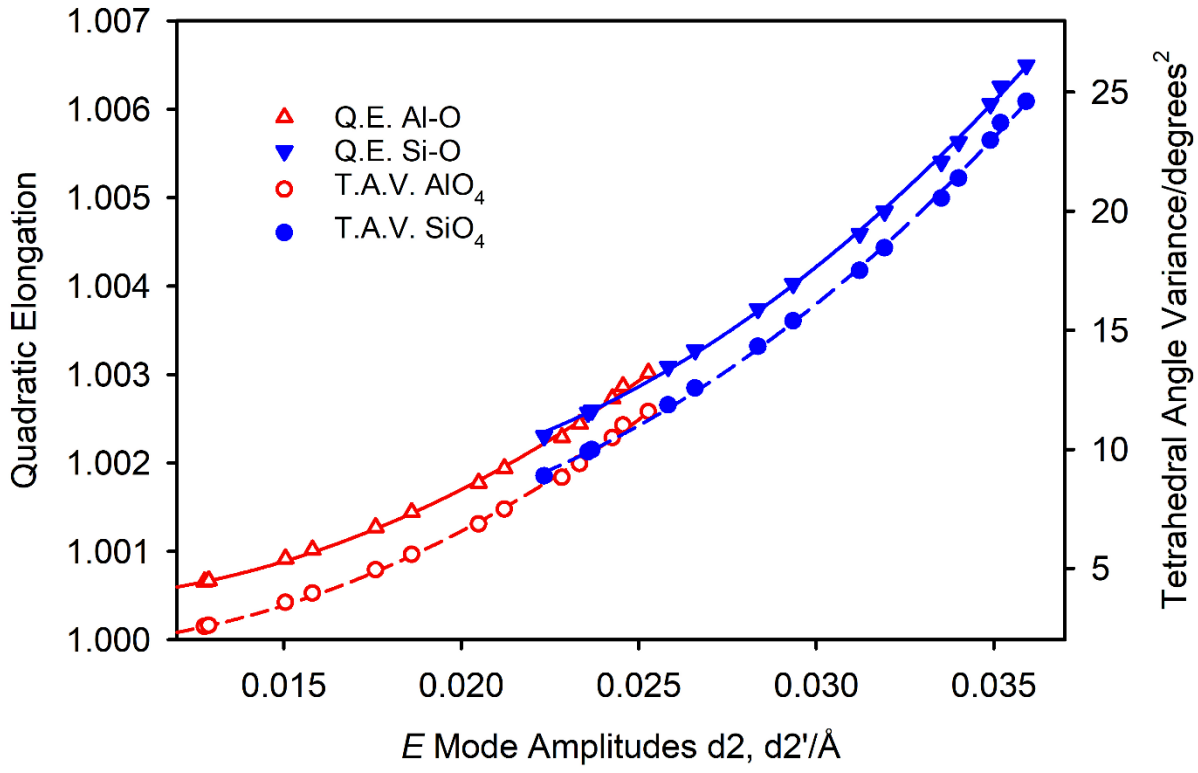

818

819 Figure 7